

UNCLASSIFIED

AD 405 123

DEFENSE DOCUMENTATION CENTER

FOR

SCIENTIFIC AND TECHNICAL INFORMATION

CAMERON STATION, ALEXANDRIA, VIRGINIA



UNCLASSIFIED

NOTICE: When government or other drawings, specifications or other data are used for any purpose other than in connection with a definitely related government procurement operation, the U. S. Government thereby incurs no responsibility, nor any obligation whatsoever; and the fact that the Government may have formulated, furnished, or in any way supplied the said drawings, specifications, or other data is not to be regarded by implication or otherwise as in any manner licensing the holder or any other person or corporation, or conveying any rights or permission to manufacture, use or sell any patented invention that may in any way be related thereto.

63-3-5

405123

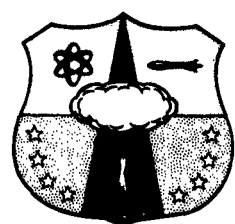
AFSWC-TDR-63-6

SWC
TDR
63-6

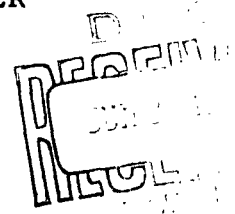
**STUDY OF THE COLLAPSE OF
SMALL SOIL-SURROUNDED TUBES**

**Interim Report
March 1963**

TECHNICAL DOCUMENTARY REPORT NUMBER AFSWC-TDR-63-6



**Research Directorate
AIR FORCE SPECIAL WEAPONS CENTER
Air Force Systems Command
Kirtland Air Force Base
New Mexico**



405123

Project No. 1080, Task No. 108001

**This research has been funded by the
Defense Atomic Support Agency under WEB No. 13.145**

**(Prepared under Contract AF 29(601)-4927 by
Ulrich Luscher, Massachusetts Institute of
Technology, Department of Civil Engineering,
Soils Research Laboratories, Cambridge,
Massachusetts)**

**HEADQUARTERS
AIR FORCE SPECIAL WEAPONS CENTER
Air Force Systems Command
Kirtland Air Force Base
New Mexico**

When Government drawings, specifications, or other data are used for any purpose other than in connection with a definitely related Government procurement operation, the United States Government thereby incurs no responsibility nor any obligation whatsoever; and the fact that the Government may have formulated, furnished, or in any way supplied the said drawings, specifications, or other data, is not to be regarded by implication or otherwise as in any manner licensing the holder or any other person or corporation, or conveying any rights or permission to manufacture, use, or sell any patented invention that may in any way be related thereto.

This report is made available for study upon the understanding that the Government's proprietary interests in and relating thereto shall not be impaired. In case of apparent conflict between the Government's proprietary interests and those of others, notify the Staff Judge Advocate, Air Force Systems Command, Andrews AF Base, Washington 25, DC.

This report is published for the exchange and stimulation of ideas; it does not necessarily express the intent or policy of any higher headquarters.

Qualified requesters may obtain copies of this report from ASTIA. Orders will be expedited if placed through the librarian or other staff member designated to request and receive documents from ASTIA.

TDR-63-6

ABSTRACT

This report describes a program of experimental and theoretical work on the problem of failure of structural tubes surrounded by a thin layer of soil loaded by uniform radial outside pressures. The properties and the thickness of the soil layer were varied, and the failure pressure of the tube, as well as the deformations of the tube before and after failure, was observed. Theories based on idealized models of the soil-structure interaction were developed. The experimental results were then correlated with these theories to determine which, if any, of the theories explained the behavior of the samples.

In addition to this work, a new testing apparatus was designed and built, in preparation for similar tests with the tube buried under a plane soil surface.

PUBLICATION REVIEW

This report has been reviewed and is approved.

Don I. Prickett USAF
DONALD I. PRICKETT
Colonel USAF
Director, Research Directorate

John J. Dishuck
JOHN J. DISHUCK
Colonel USAF
DCS/ Plans & Operations

TABLE OF CONTENTS

	<u>Page No.</u>
I INTRODUCTION	1
II THEORETICAL WORK	3
1. Introduction	3
2. Limiting Equilibrium Condition of a Soil Ring	3
3. Elastic Behavior of a Soil Ring Around a Rigid Inclusion	5
4. Over-all Buckling of a Cylindrical Shell	8
5. Buckling of an Elastically Supported Ring	10
III EXPERIMENTS AND RESULTS	12
1. Review of Previous Work	12
2. Further Tests on Aluminum Foil Tubes	13
3. Further Tests on Sand-surrounded Tubes	14
4. Tests on Grout-surrounded Tubes	15
5. Tests on Grout-sand-surrounded Tubes	17
IV DISCUSSION AND CORRELATION OF DATA	22
1. Old "Arching Theory"	22
2. "Over-all Buckling" Theory	24
3. Buckling of an Elastically Supported Ring	25
4. Conclusions	29

	<u>Page No.</u>
V. PLANE STRAIN APPARATUS	31
1. Dimensions of Soil Mass	31
2. Loading Scheme	31
3. Consideration. Relating to Sample Preparation	32
4. Special Features	32
5. Tube Supports	33
BIBLIOGRAPHY	34
LIST OF SYMBOLS	35
TABLES	37
FIGURES	45
APPENDIX A	
Stresses Around a Rigid Circular Inclusion	65
APPENDIX B	
Buckling of an Elastically Supported Ring	69
DISTRIBUTION	74

LIST OF TABLES

	<u>Page No.</u>
Table I Bare Tube Tests	37
II Sand-surrounded Tube Tests - Data	38
III Grout-surrounded Tube Tests - Data	39
IV Grout-sand-surrounded Tube Tests - Data	40
V Sand-surrounded Tube Tests - Correlation by "Arching Theory"	41
VI Sand-surrounded Tube Tests - Correlation by "Elastic Buckling" Theory	42
VII Grout-surrounded Tube Tests - Correlation	43
VIII Grout-sand-surrounded Tube Tests - Correla- tion by "Elastic Buckling" Theory	44

LIST OF FIGURES

	<u>Page No.</u>
Figure 1 Equilibrium of Soil Ring	45
2 Soil Around Rigid Inclusion - Problem	45
3 Soil Around Rigid Inclusion - Solutions	46
4 Over-all Buckling of Composite Sample	47
5 Mohr Diagram for Cohesive Soils	48
6 Buckling of Elastically Supported Ring	48
7 Buckling of Elastically Supported Ring - Results	49
8 Hollow Cylinder Tests on Sand	50
9 Failure Phenomena of Sand-surrounded Tubes	51
10 Properties of AM-9 Grout	52
11 Triaxial Test on Grout-sand	53
12 Hollow Cylinder Tests on Grout-sand	54
13 Deformations of Grout-sand-surrounded Tubes	55
14 Sand-surrounded Tubes - Correlation by "Elastic Buckling" Theory	56
15 Correlation of Mode Numbers	57
16 Drawings of Plane Strain Apparatus (5 pages)	58
17 Photos of Plane Strain Apparatus	63

INTRODUCTION

This Interim Report describes the progress of the small-scale soil-structure interaction studies conducted under Contract AF 29(601)-4927 at the Massachusetts Institute of Technology between 15 November 1961 and 15 November 1962. This research is a continuation of the small-scale soil-structure interaction studies undertaken at M.I.T. under Contract AF 29(601)-1947 under sponsorship of the Air Force Special Weapons Center. That previous work, "Preliminary Design Study for a Dynamic Soil Testing Laboratory," is described in Report AFSWC TR-61-58, Appendices K and L (Ref. (1)), and in "Basic Experiment into Soil-Structure Interaction," by R. V. Whitman and U. Luscher, ASCE Journal of the Soil Mechanics and Foundation Division, December 1962 (Ref. (2)).

The work done during this reporting period can be divided into four major phases, and the report is organized accordingly. These phases are:

(i) Theoretical work. A number of soil behavior and soil-structure interaction theories were developed in an effort to explain and correlate the experimental results.

(ii) Experimental work. This includes both supporting tests and interaction tests. Among the supporting tests were soil properties tests, tests on bare structural tubes, and tests on hollow soil cylinders without interior supporting structural tubes. In the interaction tests, structural tubes surrounded by a layer of soil were subjected to increasing outside radial pressures. The total volume changes undergone by the assembly during the test, the failure pressure, and the failure mode were observed. With the samples supported in such a way that they experienced no axial strains, the soil was in a plane strain condition. Three types of "soils" were used. The soil properties and the thickness of the soil surrounding were varied.

(iii) Correlation. The analytical theories and the experimental results were correlated to determine whether the data fit one or more of the theories.

(iv) Design of new equipment. On June 1, 1962, the original contract was extended and widened in scope to include investigation of tubes buried under a horizontal soil surface and subjected to varying ratios of horizontal to vertical pressures. The only work done so far on this phase was concerned with the provision of the necessary equipment; the plane strain testing apparatus designed and built for these new tests is described in the last chapter of this report.

As far as phases (i) to (iii) are concerned, it should be understood that the sequence of the work was not as described here, but that experimental work, development of theoretical approaches and correlation attempts went hand in hand, each contributing to the progress of the others.

As of the date of this report, the experimental and correlation work of phases (ii) and (iii) was still continuing. Thus the corresponding parts of the report will be very much in the form of a progress report on research still underway. The theoretical work of phase (i), relating to the behavior of axially symmetrical soil-structure configurations, has essentially been completed, unless it should become apparent that new theories are required to explain the observed phenomena.

The research described in this report was performed in the Soils Research Laboratories of the Department of Civil Engineering at M.I.T. The head of the soils laboratories is Dr. T. W. Lambe, Professor of Civil Engineering. The project is under the direct supervision of Dr. R. V. Whitman, Associate Professor of Civil Engineering. The author is Instructor of Civil Engineering.

II THEORETICAL WORK

1. Introduction

This chapter presents a number of theoretical derivations that have been employed in the analysis of the experimental results.

The basic problem, which is treated by various mathematical approximations, is that of the interaction between a very thin metal tube and a surrounding layer of soil of uniform thickness, acted upon by a uniform outside pressure. The ends of the tube are supported, and the length of the sample is maintained constant. Thus, if end effects are negligible at mid-length of the sample, a plane strain condition exists there.

The metal tube used in the tests is a two-ply extra-heavy aluminum foil tube of 0.003-inch total thickness and a radius of 0.812 inch. In the earlier work (Ref. (1) and (2)) 10-inch long tubes were studied and were found to buckle, when there was no surrounding soil layer, at 0.27 psi outside pressure, but to sustain up to 10 psi outside pressure when surrounded by a 3/8-inch layer of Ottawa sand. This same two-ply aluminum foil tube, and soil thicknesses of 3/16 inch and 3/8 inch, will be used in the following theoretical work whenever numerical examples are given.

2. Limiting Equilibrium Condition of a Soil Ring

The limiting equilibrium condition for active arching (compression failure) of a cohesionless soil ring was derived in Ref. (1), Appendix K. Starting out with the general equilibrium equation for stresses in a soil ring (Fig. 1), for axial symmetry of the ring and the loading,*

$$\frac{d\sigma_r}{dr} r + \sigma_r - \sigma_t = 0 \quad , \quad (1)$$

*All symbols are defined where they first appear, and additionally in the "LIST OF SYMBOLS."

where $\bar{\sigma}_r$ = radial stress
 $\bar{\sigma}_t$ = tangential stress
 r = radius.

Formulating

$$\lambda_a = \left(\frac{\bar{\sigma}_r}{\bar{\sigma}_t} \right)_a = \frac{1 - \sin \phi}{1 + \sin \phi}$$

where $\lambda = \frac{\bar{\sigma}_r}{\bar{\sigma}_t}$

ϕ = soil friction angle,

for an active failure condition throughout the ring, the desired relationship was obtained as

$$\left(\frac{p_o}{p_i} \right)_a = \left(\frac{r_o}{r_i} \right)^{\frac{1-\lambda_a}{\lambda_a}}, \quad (2)$$

where p_o = outside pressure

p_i = inside pressure

r_o = outside radius

r_i = inside radius.

From Figure 5, it is seen that the Mohr diagram of a soil having both cohesion (c) and friction (ϕ) can be transformed into the diagram of a cohesionless soil by a translation of the ordinate such that $p' = p + c \cot \phi = p + 2c \sqrt{\lambda_a} / (1 - \lambda_a)$. Thus, if in Equation (2) p is replaced by p' , Equation (3), valid for a soil having both cohesion and friction, is obtained:

$$\left(\frac{p_o'}{p_i'} \right)_a = \left(\frac{r_o}{r_i} \right)^{\frac{1-\lambda_a}{\lambda_a}} \quad (3)$$

$$\text{with } p_0' = p_0 + 2c \frac{\sqrt{\lambda_a}}{1 - \lambda_a}$$

$$p_1' = p_1 + 2c \frac{\sqrt{\lambda_a}}{1 - \lambda_a}$$

$$\lambda_a = \frac{1 - \sin \phi}{1 + \sin \phi}$$

Equation (3) is not valid for a purely cohesive soil ($\phi = 0$) and must be replaced by

$$p_0 - p_1 = 2c \log \left(\frac{r_o}{r_i} \right). \quad (4)$$

Equation (2), strictly speaking, is not limited to an active arching condition, but holds for any ratio $\lambda = \sigma_r / \sigma_t$ which is constant throughout the ring. Thus, the equation could be applied for "tensile" failure of the soil ring by formulating

$$\lambda_r = \left(\frac{\sigma_r}{\sigma_t} \right)_r = \frac{1}{\lambda_a},$$

which, when substituted into Equation (2) leads to

$$\left(\frac{p_o}{p_i} \right)_r = \left(\frac{r_o}{r_i} \right)^{\frac{1 - \lambda_r}{\lambda_r}} = \left(\frac{r_o}{r_i} \right)^{(\lambda_a - 1)} \quad (5)$$

which is Kirkpatrick's formula (Ref. (3)).

3. Elastic Behavior of a Soil Ring Around a Rigid Inclusion

As an approximation of the behavior of the soil around an unyielding structural tube, the "elastic" behavior of a soil ring around a rigid inclusion has been investigated.

For specific simple cases of assumed soil behavior, Equation (2) can be used to establish the relationship between outside and inside pressures. The following cases with a constant $\bar{\sigma}_t/\bar{\sigma}_r$ ratio might be of interest:

Hydrostatic case: $\frac{1}{\lambda} = \bar{\sigma}_t/\bar{\sigma}_r = 1$

"Zero tangential stress": $\frac{1}{\lambda} = 0$, since $\bar{\sigma}_t = 0$.

"At rest": $\frac{1}{\lambda} = 1 - \sin\phi$, since $\bar{\sigma}_t = K_0 \bar{\sigma}_r \approx (1 - \sin\phi) \bar{\sigma}_r$, where K_0 = coefficient of lateral soil pressure at rest $\approx 1 - \sin\phi$

"Tensile" failure: $\frac{1}{\lambda} = \frac{1 - \sin\phi}{1 + \sin\phi}$

Numerical answers for these cases have been calculated for $r_o/r_i = 1.46$ and $\phi = 37^\circ$, and are presented in Figure 3a.

If the radial and therefore the tangential strains of the tube are small compared to the strain required to mobilize any appreciable tangential soil stresses, a K_0 condition (that is, with $\bar{\sigma}_t$ as the lateral pressure at rest) immediately next to the tube is a reasonable assumption. This K_0 -stress condition, however, would exist only in the immediate vicinity of the tube, and would be modified farther away. This can easily be visualized for the case of a rigid circular inclusion in a uniformly stressed plane, in which the stresses would approach their undisturbed values at a distance from the inclusion. Thus the above at-rest solution assuming constant $\bar{\sigma}_t/\bar{\sigma}_r$ throughout the ring is a rough approximation only, which becomes progressively inaccurate for increasing ring thickness.

A plane-strain solution for the case of an infinitely rigid circular inclusion in an elastic plane equally stressed in all directions has been worked out and is presented in Appendix A. Figure 2 illustrates the problem and gives the notation. To summarize briefly the results, the differential equation for the inward radial displacement u is

$$r^2 \frac{d^2 u}{dr^2} + r \frac{du}{dr} - u = 0. \quad (6)$$

The solution, for the boundary conditions $u(r_i) = 0$ and $u(r_o \rightarrow \infty) = u_o$, is

$$u = r \frac{\sigma_o}{E_s} (1 - \nu - 2\nu^2) \left[1 - \left(\frac{r_i}{r}\right)^2 \right], \quad (7)$$

where σ_o = equal stress in all directions of the plane

E_s = modulus of elasticity of soil

ν = Poisson's ratio of soil,

and the resulting stresses are

$$\begin{aligned} \sigma_r &= \sigma_o \left[1 + \left(\frac{r_i}{r}\right)^2 (1 - 2\nu) \right] \\ \sigma_t &= \sigma_o \left[1 - \left(\frac{r_i}{r}\right)^2 (1 - 2\nu) \right] \\ \sigma_a &= 2\nu \sigma_o \quad (\text{in axial direction}). \end{aligned} \quad (8)$$

The stresses are plotted in Figure 3b for $\nu = 0.4$, $\nu = 0.3$ and $\nu = 0.286$. The last value is of interest because it yields an "at rest" condition with $\sigma_t/\sigma_r = 0.4 = K_o$ next to the inclusion. Using $\nu = 0.286$ and a soil ring with $r_o/r_i = 1.46$, the ratio of p_i/p_o becomes 1.19, as compared to 1.26 for the approximate solution assuming a constant ratio of σ_t/σ_r equal to 0.4 throughout the ring.

A correction was made for the case of an assumed displacement of the tube (based on experimental data) of $u_i = 0.0005$ inch by substituting this value as boundary condition into the solution of the differential equation. For $E_s = 400 \sigma_o$ and $r_o/r_i = 1.46$, this resulted in $p_i/p_o = 1.11$.

Thus, an exact solution has been obtained for the case of an infinitely rigid circular inclusion in a uniformly stressed plane. The radial and tangential stresses vary at an appreciable rate with distance from the inclusion,

and therefore the approximate solution assuming a constant stress ratio is valid only for very thin soil rings. From the exact solution, ratios of inside to outside pressures for soil rings around unyielding cylinders can be obtained. Moreover, a small inward displacement of the cylinder can be approximately considered and, as expected, somewhat reduces the stress concentration around the inclusion.

4. Over-all Buckling of a Cylindrical Shell

The formula for buckling of a simply supported cylindrical shell under radial outside pressure is given in Timoshenko (Ref. (4)) as

$$P_{cr}/E = \frac{h}{r(n^2-1)\left(1 + \frac{n^2 L^2}{\pi^2 r^2}\right)^2} + \frac{h^3}{12r^3(1-\nu^2)} \left(n^2 - 1 + \frac{2n^2 - 1 - \nu}{1 + \frac{n^2 L^2}{\pi^2 r^2}} \right), \quad (9)$$

where P_{cr} = critical buckling pressure

E = modulus of elasticity of tube material

n = number of modes

h = thickness of tube

L = length of tube.

For a long tube, this reduces to the simple formula

$$P_{cr}/E = \frac{h^3 (n^2 - 1)}{12r^3 (1 - \nu^2)}. \quad (10)$$

For thin soil rings of low modulus of elasticity surrounding a structural tube, over-all buckling of the sample may be the controlling mode of failure. To check this, the formula for buckling of a shell with a non-homogeneous cross section has to be found. It is seen that the first term of Equation (9) is proportional to the shell thickness h , the second term proportional to the moment of inertia I . By inference, therefore, the buckling formula for a non-homogeneous cross section might be written as

$$p_{cr}/E = \frac{h'}{r'(n^2-1)\left(1 + \frac{n^2 L^2}{12 r'^2}\right)^2} + \frac{I'}{r'^3} \left(n^2 - 1 + \frac{2n^2 - 1 - \nu}{1 + \frac{n^2 L^2}{12 r'^2}} \right), \quad (11)$$

where h' = equivalent tube thickness = $\sum h_j \frac{E_j}{E}$

I' = equivalent moment of inertia

$$= \sum I_j \frac{E_j}{E} = \sum \frac{h_j^3}{12(1-\nu^2)} \frac{E_j}{E}$$

r' = radius to center of gravity of section

j (subscript) = concerning the j th layer.

In this formulation, no bond stress is assumed to act between the individual layers; however, this assumption has to be verified in each case. The ν in the last numerator has very little influence for n over 2 and may be given an average value.

Using as specific example the two-ply aluminum foil tube of 0.003-inch total thickness, surrounded by soil with a modulus of elasticity below 40 psi and with a maximum thickness of 0.375 inch, it follows that $h' \approx h$ and $r' \approx r_{al}$. Thus the presence of the soil is felt only in the inertia term.

Curves of p_{cr}/E_{al} ($E_{al} = E$ of aluminum) versus n were calculated and plotted for soil thicknesses h_s (around the aluminum foil tube) of 0.188 inch and 0.375 inch, and moduli of elasticity of soil E_s of 6.7, 15 and 30 psi. The minima of the curves yielded $(p_{cr}/E_{al})_{min}$ and n_{cr} (the critical mode number), whereby it was stipulated that n_{cr} need not be an integer, but is that value leading to $(p_{cr}/E_{al})_{min}$. The results are presented in Figure 4a, where $(p_{cr})_{min}$ is plotted versus E_s for the two soil thicknesses, and in Figure 4b, where $(p_{cr}/E_{al})_{min}$ is plotted versus I' . This last plot is only possible because the first term of Equation (11) is independent of the soil surrounding.

5. Buckling of an Elastically Supported Ring

In connection with the failure of a flexible tube surrounded by a layer of soil, it appears pertinent to consider the problem of buckling of a ring subjected to large compressive forces and elastically supported against deformation (i.e., with counteracting radial forces proportional to the radial deformation). This problem is analogous to the buckling of a laterally supported column.

The mathematical approach to this problem is similar to a derivation in Hetenyi (Ref. (6)), pp. 156-159, except that here the equilibrium equations must be formulated not for the original, but for the deformed geometry, to allow for an instability condition. The problem is presented in Figure 6, and the detailed derivations are reproduced in Appendix B.

The resulting differential equation for the ring deformation is

$$\frac{d^5 y}{d\psi^5} + (2 + \bar{p} a) \frac{d^3 y}{d\psi^3} + (kra + 1) \frac{dy}{d\psi} = 0, \quad (12)$$

where y = ring deflection (outward positive)

ψ = central angle

$a = r^3/EI$, with r , E and I being properties of the ring

k = coefficient of elastic soil reaction

\bar{p} = average pressure applied on the ring.

Formulating a periodic buckled form as $y = B \sin n\psi$, the following equation results:

$$n^5 - n^3(2 + \bar{p} a) + n(kra + 1) = 0 \quad (13)$$

This equation was solved for \bar{p} in terms of n , was minimized with respect to n , and yielded the approximate solution

$$\bar{p}_{cr} = 2\sqrt{\frac{kr}{a}}, \quad (14)$$

which is valid for all practical values of k . Similarly, an expression for n_{cr} was obtained as

$$n_{cr} = \sqrt[4]{kra} \quad (15)$$

For the two-ply aluminum foil tube as structural member, these relationships are presented in Figure 7, which is a plot of the critical tube buckling pressure \bar{p}_{cr} versus the modulus of soil reaction k . Also indicated on the figure are the critical mode numbers n_{cr} .

III EXPERIMENTS AND RESULTS

1. Review of Previous Work

Experimental work dealing with sand-surrounded tubes had already been done in the years 1959-1961 and is reported in Appendices K and L of Reference (1). A further reference describing that research (Ref. (2)) includes results up to November 1961 and gives some new interpretations.

The first part of this previous effort dealt with the behavior of hollow sand cylinders (Figures 1 and 8). The theory (which is repeated in Chapter II, 1 of this report) indicated that a hollow sand cylinder, of given geometry and with given friction angle, should collapse when the ratio of outside to inside pressure reaches a certain critical value. The experiments confirmed the validity of this theory, except that the effective friction angle was considerably higher than that obtained from triaxial tests on identical samples. Presumably this discrepancy resulted from the different straining conditions in the two types of tests, which is in agreement with observations by others, e.g. Kirkpatrick (Ref. (3)) and Bjerrum (Ref. (7)).

After extensive search, a two-ply aluminum foil tube was chosen as the structural tube. It was manufactured by rolling two layers of extra-heavy aluminum foil, 0.0015 inch thick, over a mandrel. The layers were bonded together by shellac or rubber cement. These tubes, of a total thickness of 0.003 inch and a diameter of 1.625 inch, were found to buckle consistently both under a radial pressure and with a deformation pattern in reasonable agreement with predictions based on the theory for the buckling of cylindrical shells (Eq. (9) of Chapter II, 3). However, the backcalculated modulus of elasticity was only 4.5×10^6 psi.

Finally, tests on sand-surrounded tubes were undertaken. The outside pressure necessary to collapse these composite samples (with zero inside pressure and zero pore pressure) was much greater than that which would buckle the bare tubes. Using the results obtained for the hollow sand cylinders, it was found that soil arching alone could account for only a small portion of this increase.

Special tests were performed in which part of the pressure was applied to the tubes as pore pressure in the surrounding soil. From the results of these tests, and again using the soil arching theory, it was shown that the tubes, when surrounded by sand, had a restrained-buckling strength approximately ten times greater than the buckling strength of the bare tube. This restrained-buckling strength was more-or-less independent of the thickness and density of the surrounding sand. Highly puzzling was the fact that deformation measurements for the sand cylinders alone, for the tubes alone, and for the sand-surrounded tubes indicated that the strain of the sand ring at compression failure would have to be about 100 times greater than the strain of the tube at failure. Yet apparently the full strength of each was mobilized in the sand-surrounded tube tests.

It is seen from this short summary of previous work that, while much useful information had been obtained, a number of phenomena remained unexplained. This fact, along with the desire to include other types of soil and, possibly, other types of tubes, prompted the continuation of the research as described in the following sections.

2. Further Tests on Aluminum Foil Tubes

Additional tests on bare aluminum foil tubes were run to eliminate, if possible, the apparent discrepancy between the backcalculated and the conventional modulus of elasticity of the tube material (4.5×10^6 psi versus 10×10^6 psi). Tubes with two different lengths, 10 inches and 6 inches, and three thicknesses, one-ply, two-ply and three-ply, were tested. The failure pressure and the failure mode were observed in all tests, and average tube deformations were determined in some tests by measuring, in a horizontal capillary tube, the amount of water displaced out of the water-filled aluminum foil tube.

The results of these tests, presented in Table I, were correlated with the cylindrical shell buckling theory. Equation (9), when minimized for p_{cr}/E in terms of n , yields, for a given situation, a critical buckling value $(p_{cr}/E)_{min}$ and a critical buckling mode n_{cr} . With experimental results

expressed in terms of observed p_{cr} and n_{cr} , the modulus of elasticity necessary to explain the buckling resistance can be backcalculated, and the mode numbers compared (see also Ref. (2)). The correlation was made both for the "full bond" theory of tube action, where it was assumed that full shear forces were transmitted across the glued joint(s), and for the "no bond" theory, which assumed no bond stress at all to act between the plies. These calculations are also presented in Table I.

It becomes apparent from the table that the "no bond" theory is most nearly correct, as it leads to good agreement between theory and experiment. The fact that the backcalculated modulus is somewhat too high in all cases of multi-ply tubes must be due to some shear being transmitted across the glued joint, and to some fixation at the ends not considered in the theory, which assumes "simple" end supports.

In conclusion, the agreement between theory and experiments was good if the tubes were hypothesized to act as series of unconnected single-ply tubes. Apparently the glue was much too soft in comparison with the aluminum to force the multi-ply tube to act like a solid tube in bending.

3. Further Tests on Sand-surrounded Tubes

The additional tests described in Reference (2) on Ottawa sand-surrounded tubes were undertaken to obtain more evidence supporting the arching theory, which originally had been based on only one very limited series of tests. Later, similar tests explored the effect of the soil density upon the behavior of the sand-surrounded tubes, and are reported herein for the first time.

The testing equipment and method were as described in Reference (1), Appendix L, with two modifications as follows: First, loose sand was obtained by dropping it into standing water and tapping the mold slightly, rather than tamping the sand as described for obtaining dense sand. Since the lateral pressure of the loose sand was insufficient to push the membrane into position, a vacuum device was used to pull the membrane back against the mold. Second, a method

was devised to obtain a measure of the average radial deformation of the tube: The total volume change of the aluminum foil tube was measured in a horizontal capillary tube. This method also allowed stopping of the failure process at any desired time by closing off the outflow of water, thereby conserving the sample in a state of beginning failure for later inspection. Thus in these tests, the failure pressure and failure mode, as well as the average deformation of the tube with applied load were observed.

The data obtained in these tests are presented in Table II. For completeness, Table II includes the data already presented in Table III of Reference (2).

Failure of these soil-surrounded tubes was first recognizable by a rapid increase in the measured volume changes. If the "drainage" line was not closed, water continued squirting out of the end of the capillary tube at constant applied pressure, and eventually visible failure patterns developed in the sand, as shown in Figure 9a taken from Reference (1). Prevention of large deformations by closing the line permitted inspection and evaluation of the tube failure pattern in many tests. This pattern consisted of one or more narrow creases, as shown in Figure 9b taken from Reference (2). The portion of the tube circumference involved in a single crease or the distance between adjacent creases, divided into the circumference, was defined as the experimental mode number n .

4. Tests on Grout-surrounded Tubes

To investigate other combinations of soil-surrounded tubes, a suitable soft, plastic soil was sought. Consolidated soils were excluded from consideration because of the difficulties inherent in building a sample of the desired size and shape. The use of a compacted sample was also considered undesirable because of the complexities of its shear-strength characteristics. The search then turned to materials which could be poured and would subsequently solidify. From among these materials, AM-9 grout was chosen as the most versatile since its strength and gelling characteristics can be controlled within wide limits by the concentration of the various chemicals making up the mixture.

AM-9 is the trade name of a chemical grout manufactured and marketed by the American Cyanamid Company. Its strength characteristics are controlled by the concentration of the main chemical, AM-9. Gelling is started by the addition of a small quantity of a catalyst, and the gelling time is controlled by the concentration of a retarder which is already in solution when the catalyst is added.

In the present tests, 9 per cent and 18 per cent AM-9 concentrations were used. The amounts of the trace chemicals (which are denoted by non-chemical abbreviation) were 0.4 per cent DMAPN, 0.5 per cent AP (the catalyst), and zero per cent, 0.005 or 0.010 per cent of FeC (retarder) for approximately 2-1/2, 6, or 10 minutes of gelling time, respectively. In the tests described in this section, the grout alone was used as "soil" surrounding; grout-saturated Ottawa sand was used in another series of tests described in the next section.

To determine the mechanical characteristics of the grout, vane, unconfined compression, and hollow-cylinder buckling tests were run. The results, some of which are presented in Figure 10, may be summarized as follows:

(i) The grouts behaved as ideally cohesive materials, i.e., the confining pressure had no influence on the properties. This result suggests that the grout had no gas-filled void spaces, and hence that Poisson's ratio is 0.5.

(ii) The modulus of elasticity was 30 psi for the 18 per cent solution and 6.7 psi for the 9 per cent solution.

(iii) The shear strengths of the two grouts were appreciably different in the vane and the unconfined compression tests. In the vane tests, they were 360 psf and 100 psf; in the unconfined tests, 680 psf and 144 psf, for the stronger and weaker solution, respectively.

Two wall thicknesses and two grades of grout were used in the grout-surrounded tube tests. The samples were prepared and tested like the samples using loose sand, also employing a vacuum arrangement to pull the membrane back.

Further, since after failure of the aluminum tube the grout cylinder was still in excellent condition, it was slipped over a fresh tube and re-used in a second test. During the slipping-on, the new tube was supported by a tightly fitting inside mandrel. No systematic difference between the two tests with the same grout cylinder could be detected; in fact, the results were generally very similar. After the second test, the grout cylinder could still be used in a hollow "soil" cylinder buckling test.

Failure apparently took place in the form of over-all buckling of the sample, with one buckle developing initially, followed by others if more water was allowed to flow out of the tube.

The results of these tests, in terms of failure pressure, failure mode, and average radial deformations during the test, are presented in Table III. The strengths were very low compared to the strengths of the sand-surrounded tubes, as could intuitively be expected for this less competent "soil" surrounding. Consistent with this, the width of the buckles was much larger in these tests than in the tests using sand. The average radial deformations, on the other hand, both as far as initial slope and final value are concerned, were quite similar to those observed in the tests with sand.

5. Tests on Grout-sand-surrounded Tubes

Because of the low strength of the AM-9 grout alone and the associated apparent tendency of the grout-surrounded tubes to fail in over-all buckling, a stronger "soil" with cohesive properties was desired for use as tube surrounding. The choice fell on 9 per cent AM-9-saturated Ottawa sand as basically fulfilling the specifications set forth at the start of the previous section, notably that of pourability. This material, which will henceforth be called grout-sand, was prepared by pouring AM-9 of relatively long gelling time into the mold, adding and tamping the sand while the solution was still liquid, and letting the mixture gel. The void ratio of the soil was around 0.54.

The elastic and strength properties of this grout-sand were determined in triaxial and hollow-cylinder tests.

The triaxial tests were essentially undrained, since in the relatively short testing time (maximum 1/2 hour) no liquid was pressed out of the samples. Some of the stress-strain curves of these tests are shown in Figure 11a, and a Mohr diagram of the strength results is shown in Figure 11b. The stress-strain curves are quite steep at the very start, but flatten out very soon and maintain an almost constant slope over a large portion of the curve. The Mohr diagram suggests an overconsolidated material with a normally consolidated friction angle of 36° and a maximum past pressure of about 25 psi.

Hollow soil cylinder tests were performed in the testing apparatus used for the hollow sand cylinder tests described in Appendix K of Ref. (1). The tests were run on cylinders with 1-inch inside diameter and nominal wall thicknesses of 1/4 inch and 1/2 inch. The samples failed in a manner very reminiscent of the failure of hollow sand cylinders: compare Figure 12a to Figure 8a taken from Ref. (1). Moreover, the cohesive nature of the "soil" allowed inspection of the failed sample in cross section, shown in Figure 12b, giving conclusive proof of the failure mode hypothesized in Figure 8b, also taken from Ref. (1).

With no inside pressure, average observed outside failure pressures were 21 psi and 52 psi for the two wall thicknesses. Writing Equation (3), the equation for hollow-cylinder arching of a soil having both cohesion and friction, for each wall thickness and substituting the experimental data, two equations in c and ϕ were obtained. Simultaneous solution of the equation yielded $c = 12$ psi and $\phi = 26.3^\circ$ as the strength parameters necessary to explain the observed behavior. These strength parameters were additionally verified by tests in which 1/2-inch thick hollow cylinders failed at an inside pressure of 10 psi and an outside pressure of 83 psi. Drawing the strength envelope defined by this c and ϕ into the Mohr diagram, Figure 11b, the agreement between the two types of tests, for the pressure ranges used, is seen to be excellent, considering the fact that the cylinder-arching theory allows only two parameters c and ϕ , whereas the broken envelope resulting from the triaxial tests is more complicated.

Additional hollow cylinder data for the grout-sand, including failure pressures and phenomena at failure as well as deformations, were obtained on cylinders after they had been used in the soil-surrounded tube tests. The average observed failure pressure (neglecting premature local failures which tended to occur) of 19.5 psi for a cylinder with 0.812-inch inside radius and 0.375-inch wall thickness agreed very well with the previous data. The total average radial deformation of the inside surface at failure was approximately 0.045-inch or 5.5 per cent of the radius. Moreover, the deformation versus applied pressure curves generally exhibited a more-or-less straight portion sloped at 0.0022-inch per psi. Assuming thin-ring behavior for the median plane of the ring, this corresponds to a modulus of elasticity of 1800 psi, which is in general agreement with the moduli found in tri-axial tests.

A substantial number of tests with this grout-sand surrounding the two-ply aluminum foil tube were run. Experimental difficulties, the solution to which had to be found by trial and error methods, affected a number of the earlier tests. Moreover, the results of the tests which were considered successful still showed appreciable scatter, such that the same phenomenon had to be observed at least twice to assure the existence of a trend.

The results of all these tests are presented in Table IV. Included are the apparently unsuccessful tests (1 to 5, and 11), since some of the information gained in these tests still has potential value. Typical deformation versus pressure curves are shown in Figure 13, separated into a low and a high pressure range.

At the start of the test, the deformations remained very small, as shown in Figure 13a. At a certain pressure, however, the deformation increased suddenly by an order of magnitude, but regained an equilibrium condition at constant applied pressure. If the sample was taken out of the pressure cell at this stage and investigated, it invariably showed that the aluminum tube had failed by developing one or more buckles, even though no failure was discernible from the outside. Thus this point was defined as the "tube failure" point.

If the sample was reloaded at that time, leaving the original, buckled tube in place, it generally showed a deformation curve resembling that of Test 8, Figure 13b, reaching failure at about 19.5 psi. Such behavior is very similar to that of unsupported hollow cylinders of the same material and geometry. Two exceptions to the normal behavior were observed: see Figure 13b. Sample 6, upon reloading, showed again quite stiff behavior, up to its previously established failure pressure of 9 psi, then turned onto a steeper deformation-versus-pressure curve, and finally failed at 24 psi. Test 10, the only test which was not interrupted after tube failure, exhibited the usual phenomena up to that point, then followed a slope corresponding to "soil alone" arching action and failed at 27 psi.

To summarize the deformation data, three completely different phases were generally observed: At first, the deformations increased very slowly, amounting to about $0.04 - 0.06 \times 10^{-3}$ inch per psi initially and $0.6 - 1.0 \times 10^{-3}$ inch at tube failure, more-or-less independent of the failure pressure. At tube failure, a sudden large deformation occurred, presumably as part or all of the load originally carried by the tube was transferred to the soil cylinder. Further deformations were much larger, averaging about 1.7×10^{-3} inch per psi, indicating that the soil cylinder alone carried the extra load.

The strength results can now be summarized as follows:

(i) Premature tube failure, which was mainly due to poor quality of the grout-sand near the bottom of the sample, occurred between 1.7 and 3.6 psi outside pressure, but mostly between 2.0 and 2.7 psi outside pressure.

(ii) In good tests, the aluminum tube failed at outside pressures between 8.0 and 11.8 psi.

(iii) With the "failed" tube left inside, the sample sustained further pressure increases up to about 19.5 or 25.5 psi. Presumably the final failure occurred at 19.5 psi if the tube had failed

in such a way that it did not enhance the strength of the sample, and at 25.5 psi if the tube had failed in such a way that it continued to contribute to the resistance of the sample.

Data on tube failure modes were obtained from a number of tests. It was difficult to obtain these data, since the large deformations associated with mobilization of the soil strength after the tube failure tended to destroy the original failure mode of the tube. Thus, to get this information, the test had to be stopped after tube failure and the mode data taken before pressures could be reapplied to the sample. These data indicated a crease width of about 5 mm, corresponding to a mode number n of about 26, for tube failures between 8.0 and 11.8 psi. For premature failures at 2.0 to 3.6 psi, the crease widths averaged 11 mm, corresponding to $n = 12$.

To summarize these data of grout-sand surrounded tubes, the most important finding is that the aluminum tubes failed at pressures which were in all cases below the failure of the surrounding soil alone. Thus failure of the tube did not initiate over-all failure, but constituted merely the stage in the process of mobilization of resistance at which the stiffest component failed, since it acted in a brittle fashion. The sample as a whole sustained higher stresses which in general equalled the failure pressure of the soil cylinder alone, but showed definite indications in two cases that the aluminum tube, even in its "failed" state, helped to sustain loads.

IV DISCUSSION AND CORRELATION OF DATA

This chapter will attempt to bring together the three sets of data using the theories presented in Chapter II in order to show how well these theories explain the results and what discrepancies there are.

1. Old "Arching Theory"

An arching theory was developed in the earlier work described in Ref. (1) and (2), which appeared to explain the data of the sand-surrounded tube tests very well. This theory assumed that the full arching strength of the sand was mobilized around the tube. With this hypothesis, the backcalculated tube strength was consistently around 2.5 psi for a variety of tests, which at the time seemed to prove the theory.

(a) Sand-surrounded tubes

In Table V are presented the results of an evaluation of the more recent sand-surrounded tube tests by the arching theory. The buckling mode number n for a critical pressure of 2.5 psi was obtained from Equation (10) as 15 for unsupported buckling of the tube.

While a critical tube-buckling pressure of 2.5 psi ± 15 per cent was again obtained quite consistently, a number of drawbacks and serious uncertainties were evident.

(i) As yet, there is no independent explanation of why the restrained tube-buckling pressure should be 2.5 psi, independent of the sand thickness or density.

(ii) Two tests (20 and N3) showed higher failure pressures (by about 50 per cent and 90 per cent) than could be explained by the arching theory and the constant critical tube buckling pressure of 2.5 psi. While postulation of higher mode failures could conceivably explain these data, it appears strange that the higher modes should occur in connection with the thin soil surrounding rather than the thicker one.

(iii) The evidence from comparison of buckling modes is inconclusive, mainly because most of the observations were for special tests with high pore pressures, for which the buckling mode seemed to be about 10. Only two contradictory observations exist for normal tests, one of $n = 11$, the other of $n = 26$ for the test exhibiting exceptionally high strength.

(iv) Most seriously, a strain discrepancy existed, in that the strains deemed necessary to develop full arching in the soil (determined from modulus of elasticity considerations as well as from measured deformations in the hollow sand cylinder tests) were roughly 100 times higher than the strains actually measured at failure of the samples. An explanation advanced in Ref. (1) Appendix L, which involves the difference of the stress histories of the sand in soil-surrounded tube tests and hollow soil cylinder tests is unsatisfactory in view of the order of magnitude of the discrepancy.

(b) Grout-surrounded tubes

Grout-surrounded tube samples failed in a manner strongly suggesting an over-all buckling failure. Moreover, inspection of the sample showed that the grout obviously did not fail in shear. Thus it has to be concluded that the arching theory does not pertain to these tests.

(c) Grout-sand-surrounded tubes

Finally, it becomes evident that the grout-sand-surrounded tube tests cannot be fitted to the arching theory. For while the outside pressures associated with failure of the tube were in the same range as the highest pressures measured in sand-surrounded tubes, at that pressure only the tube (but certainly not the grout-sand) had developed its full potential. This was clearly shown by the rapid increase in deformation after tube failure, which indicated that the load was transferred from the failing tube to the soil, and by the much

higher failure pressure of the sample as a whole.

Thus it has been proven that at least for this grout-soil-tube configuration, the combined strength of the soil and the tube was not attained, but that the tube failed first because of its brittleness. Contradicting this statement, however, are the two tests (S6 and S10) in which, even after deformations as large as 5 per cent, the tubes seemed to contribute to the strength; this suggests the validity of the arching theory for a "large-deformation" condition in certain cases.

(d) Conclusion

It is concluded that the drawbacks of the arching theory are severe indeed, and that determined efforts should be made to find new theories to explain the data of the tests on soil-surrounded tubes.

2. "Over-all Buckling" Theory

Since it appeared that over-all buckling of the sample was the controlling mode of failure of the grout-surrounded tubes, the theory for this situation has been worked out in Chapter II and numerically applied to the wall thickness and moduli of elasticity of the grout.

Table VII compares observed values and values predicted by this theory for the failure pressure and the buckling mode of the grout-surrounded tubes. The following can be deduced from this comparison:

Very good agreement, both of critical pressures and failure modes, exists for the 0.188-inch grout surrounding, concurring with the observed impression that this type of failure was indeed the controlling one in these tests. The agreement may be further improved if the rubber membrane is included in the grout thickness, as was done in Reference (2) for the sand-surrounded tubes. Then the predicted critical pressures would be 0.59 and 1.23 for the two grades of grout.

For the 0.375-inch grout thickness, the theoretical and experimental values disagree. The observed failure pressure is lower than predicted and the mode number is higher. A probable cause of the disagreement is the fact that the simple buckling theory is only a rough approximation for thick rings, and for a combination of materials of such radically different properties (the moduli of elasticity are in a ratio of roughly $10^6:1$). The errors attributable to both these uncertainties would be larger for the thicker than for the thinner soil surrounding. It is therefore conceivable that the good agreement for 0.188-inch grout thickness was purely a fortuitous result of cancelling errors, and that this type of failure mode is actually the controlling one for both wall thicknesses. On the other hand, the disagreement for the 0.375-inch wall thickness may be an indication that the failure mode is changing or has changed to a different mode. This question cannot be treated here, but will be taken up later.

In conclusion, there are strong indications that this failure theory is valid for failure of the tube combined with thin rings of extremely soft material. For any other soil surrounding, the critical buckling pressure for this failure mode would be extremely high, so that other types of failure would occur first.

3. Buckling of an Elastically Supported Ring

This interaction theory hypothesizes:

(i) The soil around the tube behaves very much like an elastic medium around a rigid circular inclusion. The condition is somewhat modified by small deformations of the inclusion.

(ii) Tube failure occurs in the form of buckling of an elastically supported ring.

Hypothesis (i) allows calculation of the pressure acting on the tube from the known outside pressure, by the elastic behavior theory developed in Chapter II and based on the "elastic" properties of the soil. Then the coefficient of soil reaction k and the failure mode number n can be

calculated from the known tube-failure pressure. The mode number n can be compared to the available data on failure modes, and k can be correlated with the test conditions, i.e., soil type and density, wall thickness and soil effective pressure. The criteria for the applicability of the theory are agreement of observed and backcalculated mode numbers and, ultimately such good correlation of the elastic soil constant k to the test parameters that k could be predicted correctly for different parameters.

(a) Sand-surrounded tubes

Based on the calculations in Chapter II, the parameters of the elastic soil ring action were chosen as

$$\bar{p}_i/\bar{p}_0 = 1.15 \text{ for } 0.375\text{-in. sand thickness}$$

$$\bar{p}_i/\bar{p}_0 = 1.09 \text{ for } 0.188\text{-in. sand thickness}$$

Thus the soil inside pressures \bar{p}_i were calculated from the known \bar{p}_0 , and $p_i = p_{cr} = \bar{p}_i + u$. The k and n corresponding to the elastically supported tube buckling theory were then calculated by Equations (14) and (15). The results of these calculations are shown in Table VI.

Since the straining characteristics of a sand are strongly dependent upon the effective pressure in the sand, the resulting k and n values were then plotted versus \bar{p}_i (Figure 14). Unfortunately, for all "normal" tests, i.e., tests without pore pressures acting on the tube, k and n were calculated from \bar{p}_i in the first place. Consequently, the solid-line curves of Figure 14 are just curves of the mathematical relationships of k and n to \bar{p}_i over the range of the "normal" tests, and represent experimental evidence only for the range of the "special" tests, i.e., tests in which part of the pressure applied to the tube was in the form of pore pressure. The location of the points along the curves (i.e. whether \bar{p}_i was large or small), does represent experimental evidence.

Comparing experimental and theoretical mode numbers (in Table VI and Figure 15), reasonably good agreement is found in all cases. Three of these cases had a theoretical n of 12 and an average observed n of 10, one was 16 versus 11, and one 22 versus 26. More data, especially from tests with high mode numbers, would be desirable. One additional observation of a high mode number not recorded in Table VI, is the one shown in Figure 9b, but unfortunately it is not known for certain whether it is from Test 20 or 22.

(b) Grout-sand-surrounded tubes

For this soil, the outside and the inside pressures on the soil ring were taken as the same because of an estimated Poisson's ratio of close to $1/2$. Thus the calculation of k and n from the tube failure data shown in Table VIII, is based directly on the observed outside pressures of Table IV.

Since the pore pressures in these tests were unknown, the evaluation is in terms of total stresses, and all points in the plots of k and n versus p_i would be on the theoretical curves, bunched in one group for the successful tests and in a second group for the premature failures. The comparison between theoretical and observed mode numbers in Table VIII and Figure 15 is very gratifying. While individual differences are appreciable, probably mainly because of difficulties in measuring the crease widths accurately, a high and a low group, corresponding to the two classes of observed failures, are clearly distinguishable, and all data points fall into the right group.

(c) Grout-surrounded tubes

Since the over-all buckling theory failed to explain satisfactorily the behavior of the tube with a 0.375-inch grout surrounding, this situation was also considered in the light of the "elastically supported tube buckling" hypothesis. The result of the computations is shown in the last two columns of Table VII.

The resulting k values are extremely low, which might have been expected for a tube-supporting material as soft as these grouts. Comparison of the mode numbers reveals, however, that the calculated values are appreciably higher than the observed ones. Since the n values calculated from the over-all buckling theory are lower than observed, one explanation of the behavior of these samples might be that it represented a transition from the over-all buckling to the elastically supported tube buckling type of failure.

(d) Summary

The application of the elastically supported tube buckling theory to the strength behavior of the sand and grout-sand-surrounded tubes showed great promise and, furthermore, did not lead to any major discrepancies. On the other hand, a number of points require further clarification:

(i) Upon what is the coefficient of soil reaction k dependent? The evidence indicates that it was more-or-less independent of the soil density, that it was in the same range of values for sand and sound grout-sand tubes, but that it varied greatly with the soil effective pressure in the "special" sand tests, and with the soil soundness in the grout-sand tests.

(ii) While the theoretical and observed mode numbers n showed quite good agreement, the bunching of the observed values into a high and a low group, without intermediate values, seems significant and, in fact, represents a deviation from the theoretical results. As far as the sparse data indicate, this phenomenon was observed both in the sand and the grout-sand tests. In the sand tests, "special" tests with a large fraction of the applied pressure in the form of pore pressure fall into the low- n group. The others, i.e., "normal" tests and "special" tests with low pore pressures, fall into the high- n group. Among the grout-sand tests, all low- n failures fall into the group classified as "premature failures,"

induced by a weakening of the grout-sand at the sample bottom due to faulty production of the sample; failures with sound grout-sand were all of the high-n type. This fact that only high-n and low-n failures, but none in between, were observed, points out the strong tendency not considered in the theory in its present form, of the tube to fail in certain preferred modes.

(iii) The same bunching was also observed for the backcalculated coefficient of soil reaction k , especially in the grout-sand tests.

4. Conclusions

It should again be emphasized that this is an interim report on studies which are as yet unfinished. One important result of the preparation of the report has been to clarify where we stand in our understanding of the problem, and to point the way to future studies. The following paragraphs contain the tentative conclusions reached at this time.

The thin-walled grout-surrounded tubes failed in over-all buckling. Thick-walled grout-surrounded tubes deviated appreciably from that type of behavior. The deviation may have been due to gross inaccuracies in the theory for cylinders as thick as these, or, since the deviation seemed to be in the direction of elastically supported tube buckling, the failure may have represented a transition between the two types of failure.

The sand and grout-sand-surrounded tube failures have been correlated with both the arching and the elastically supported tube-buckling theories. Since each of these correlations has its strong and its weak points, the question of whether any of these theories, a combination of them, or possibly still another theory is applicable, is undecided at this time.

Ultimate failure of the grout-sand tubes was described either by the hollow cylinder strength theory (soil alone acting) or by the large deformation arching theory,

the latter in cases when even the failed tube seemed to help in sustaining the load up to ultimate failure.

V PLANE STRAIN APPARATUS

In a new phase of the research on soil-surrounded tubes, it is desired to test tubes buried under a horizontal soil surface. The new testing device designed and built for this purpose is described in this chapter of the report. Design drawings and photographs of the finished device are shown in Figures 16 and 17.

1. Dimensions of Soil Mass

The same tube will be used for these tests as was used in the symmetrical soil-surrounded tube tests. This tube has a diameter of 1.625 inch, and was tested with 6-inch and 10-inch lengths. Considering the situation of the buried tube in cross section, to minimize the effects of the soil boundaries on the behavior of the tube, soil dimensions of five times the tube diameter are widely used and were chosen here, resulting in a soil area of 8 x 8 inches. On the other hand, for a tube of a length of four to five times the diameter, the effects of the end conditions on the phenomena at mid-length are negligible. Thus, since the tube can be as long as the soil mass, a soil length of 8 inches is sufficient and thereby a cubical soil mass of 8-inch side length was chosen.

2. Loading Scheme

One design specification was that the device should allow independent control of the pressures and/or displacements on as many faces of the soil mass as was feasible. To this end, various schemes of loading by pistons and by pressurized rubber bags were considered. It was found that rubber bag loading has a number of advantages: The exact distribution of the pressure is known--it is uniform. Further, a tube can be buried close to the loaded surface without danger of load concentrations on the surface (positive or negative) due to the presence of the tube. Finally, the soil can move freely without any side friction developing. One important disadvantage is, however, that deformations cannot be measured as easily as with a piston loading arrangement. Nevertheless, it was found desirable to use rubber bag loading on as many faces as was practicable.

The final design of the device represents a compromise between what would be desirable and what it is possible to build and operate efficiently. Basically the device is a rigid closed box designed to contain a soil sample of cubical shape, 8 x 8 x 8 inches. For future reference, the three sets of faces are called top and bottom, sides, and ends, respectively; the position of the tube is imagined to be horizontal, parallel to the sides and consequently perpendicular to the ends.

One set of faces, the ends, are unyielding, thus creating a plane strain condition in the plane perpendicular to the tube axis, as was the case in the soil-surrounded tube tests. The load on these faces cannot be measured.

The top of the soil sample is loaded by a pressurized bag to ensure uniformity of pressure. It is possible to measure vertical deflections of the top either by inserting small rods through the top plate to make contact with the membrane, or by measuring the total amount of water being pressed into the bag as a measure of the average deflection, as has been done up to now for the tube interior. A rigid plate bounds the soil at the bottom. The sides of the soil cube are loaded by pressurized bags.

3. Considerations Relating to Sample Preparation

For preparation of the sample, one end piece is removed and the box is oriented with the open face up. The tube is then in a vertical position, guaranteeing uniform soil conditions all around it. Since the pressure on the top face will always be equal to or larger than the side pressure, no allowance has to be made for outward displacements in that direction; consequently the membrane can rest against the top plate during placement of the soil and will separate from it upon application of the load. Conversely, lateral expansion has to be allowed on the sides; to make this possible, the side membranes are backed up by thin Lucite plates during placement of the sand, and the plates are retracted after a positive pressure to hold the sample in place has been applied to the bags.

4. Special Features

Reduction of the friction forces on the rigid faces

is attempted by means of rubber membranes and silicon grease between the membranes and the wall. This method was used with excellent results by Dr. Rowe at the University of Manchester, England (private communication). The method is employed on the box bottom to allow unrestricted lateral expansion, and on the box ends to allow vertical deformations to develop without mobilization of high vertical shear stresses causing a loss in vertical load.

To check upon the effectiveness of the friction reducing arrangements, the box bottom is designed as a load cell consisting of two plates separated by four strain-gaged legs. This load cell checks how much of the load applied at the top arrives at the bottom; it thus indicates how much is lost because of side friction and allows experimenting with other friction reducing procedures should the one planned prove unsuccessful.

The three rubber bags are shaped essentially in the form of a closed box, with a large hole in the middle of one face. They are made either by cutting and rejoining sheet-rubber (called dental dam) into the desired shape, or by repeatedly dipping a Lucite block into a Latex solution. All bags are connected to the box in such a way that the seals do not have to be broken in each test.

The "slider assemblies" shown in Figure 16A and 16D separate the top and the side bags from each other. The assemblies have to be moved during the test by the same amount as the rest of the sides move to eliminate any lateral constraint of the sample.

5. Tube Supports

The tube supports have been thought out only far enough to prove their feasibility, but have not yet been designed in detail. Two basic types are considered. For the first type, the tubes are closed and sealed at the ends, but are connected to the outside by a thin plastic tube. This allows application of positive or "negative" pressures to the inside of the tube and measurement of volume changes as a reflection of the tube deformation. A second solution is to support the tube by thin Lucite rings at the ends; holes are provided in the box ends to observe and measure directly the deformations of the tube.

BIBLIOGRAPHY

- (1) Contract No. AF 29(601)-1947, "Preliminary Design Study for a Dynamic Soil Testing Laboratory." Report AFSWC TR-61-58 contains Appendices K, L, M and N to the final report for this project.
- (2) R. V. Whitman and U. Luscher (1962), "Basic Experiment into Soil-Structure Interaction," ASCE Jr. of the Soil Mech. & Found. Div., Dec. 1962.
- (3) Kirkpatrick, D. M. (1957), "The Condition of Failure in Sands," Proc. of the 4th Int'l. Conf. on Soil Mech. & Found. Eng.
- (4) Timoshenko, S. (1936), Theory of Elastic Stability, McGraw Hill Book Company, Inc., New York.
- (5) Timoshenko, S. (1941), Strength of Materials, Part II, D. van Nostrand Company, Inc., New York.
- (6) Hetenyi, M. I. (1946), Beams on Elastic Foundations, Univ. of Michigan Press, 1946.
- (7) Bjerrum, L. and Kummeneje, O. (1961), "Shearing Resistance of Sand Samples with Circular and Rectangular Cross Sections," Norwegian Geotechnical Institute, Pub. No. 44.

LIST OF SYMBOLS

- A = area of ring
- $a = \frac{r^3}{EI}$, coefficient of tube rigidity
- B = a constant
- c = cohesion
- E = modulus of elasticity, E_s of soil, E_{al} of aluminum
- h = tube thickness
- h_s = soil thickness
- h' = equivalent tube thickness
- I = moment of inertia
- I' = equivalent moment of inertia
- j = concerning the jth layer (subscript)
- k = coefficient of soil reaction
- K_0 = coefficient of lateral soil pressure at rest
- L = unsupported tube length
- M = bending moment in ring
- N = normal force in ring
- n = mode number
- n_{cr} = critical mode number
- p = applied pressure, p_i inside pressure, p_o outside pressure
- \bar{p} = average applied pressure
- $p' = p + c \cot \phi$

P_{cr} = critical buckling pressure

Q = shear force in ring

r = radius, r_i inside radius, r_o outside radius

u = radial displacement of the soil

x = circumferential ring coordinate

y = radial displacement of tube

ϵ = strain; subscripts as for σ

ϕ = friction angle

$\lambda = \sigma_r / \sigma_t$

ν = Poisson's ratio

σ = normal stress, σ_r radial stress
 σ_t tangential stress
 σ_a axial stress
 σ_o equal stress in all directions of the plane

ψ = central angle

Table I
BARE TUBE TESTS

Tube Thickness 10-3 in.	Tube Length (inches)	No. of Tests	Observed		Theoretical					
			Failure Pressure psi	Mode No. n	"No Bond"		"Full Bond"			
					Pcr/E 10 ⁻⁹	Back- E calculated 10 ⁶ psi	n	Pcr/E 10 ⁻⁹	Back- E calculated 10 ⁶ psi	n
1.5	6	2	0.16	5	18	8.9	5	-	-	-
3	10	8	0.27	3-4	21	12.9	4	60	4.5	3.25
3	6	3	0.43	5	37	11.6	5	101	4.25	3
4.5	6	3	0.62	5	55	11.3	5	289	2.2	4

Tube Thickness 10-3 in.	Tube Length (inches)	Observed Deformations		Theoretical Deformations	
		Initial 10-3 in/psi	Final 10-3 in.	Initial 10-3 in/psi	Final 10-3 in/psi
3	10	0.23	0.23	0.022	0.022
3	6	0.20	0.22	0.022	0.022
4.5	6	0.053	0.09	0.015	0.015

Table II

SAND-SURROUNDED TUBE TESTS - DATA

Test No.	Type of Test Normal Special	Soil Thickness (inches)	Initial Void Ratio	Outside Effective Pressure on Sand \bar{p}_o psi	Soil Pore Pressure u psi	Deformations		Failure Mode n
						Initial Δr 10^{-3} in/psi	Final Δr 10^{-3} in.	
17	N	0.188	0.54	4.65	-			9-10
18	N	0.188	0.55	4.40	-			
19	S	0.188	0.545	1.39	2.14			
20	N	0.188	0.55	7.64	-	0.019	0.29	
22	N	0.375	0.53	9.25	-			~10
24	S	0.375	0.53	5.50	1.20	0.022	0.39	
26	S	0.375	0.53	1.00	2.60	0.032	0.45	
N2	N	0.188	0.57	5.47	-			11 ~26 12
N3	N	0.188	0.57	9.6	-			
N5	S	0.188	0.57	1.45	1.71	~0.034	0.40	
N7	S	0.188	0.58	3.81	0.47	~0.068	0.48	
N23	N	0.375	0.59	9.7	-			9
N25	S	0.375	0.605	4.87	0.77	0.039	~0.44	
N26	S	0.375	0.60	0.78	2.20	0.031	~0.68	
						0.034	0.15	

Table III
GROUT-SURROUNDED TUBE TESTS - DATA

Test	Wall Thickness (inches)	AM-9 %	Failure Pressure		Tube Deformations		Failure Mode	Comments	Averaged Failure Pressure psi
			Tube Failure psi	Over-all Failure psi	Initial 10-3 in./psi	Final 10-3 in.			
A			1.50	1.60	0.041	0.25	-	10" length (all others 6")	
B1			?	2.00	-	-	-		
B2	3/8	18	0.6	1.85	0.20	0.37	8(?)	Tube damaged	1.95
C1			2.0	2.00	0.072	0.32	4-1/2		
C2			1.57	1.90		0.25			
D1			0.80	0.80	0.028	0.17	5		0.81
D2	3/8	9	0.82	0.82		0.20			
E1			0.52	0.52	-	-	-	Tube damaged	0.59
E2	3/16	9	0.59	0.59	0.120	0.22	5		
F1			1.33	1.33	0.100	0.30	4		1.32
F2	3/16	18	1.30	1.30	0.110	0.48	3.7		

Table IV
 GROUT-SAND-SURROUNDED TUBE TESTS - DATA
 (2nd loading denoted by a, 3rd loading by b)

Test No.	Void Ratio	Length L (inches)	Tube Failure			Over-all Failure		
			po (psi)	Initial Δr (10-3 in./psi)	Final Δr (10-3 in.)	Failure Mode	po (psi)	Final Deformation (10-3 in.)
1	-	10	-	-	-	-	10	-
2	0.54	10	2.0	0.032	0.22	Crease	20	-
3	0.54	10	-	-	-	-	-	-
3b	0.54	10	2.7	0.026	0.11	11 mm crease	19	~30
4	0.54	10	2.0	-	0.47	10 mm crease	-	-
5	0.55	10	1.7	-	0.48	12 mm crease	-	-
6	0.53	6	9.0	-	-	Narrow creases	-	-
6a	0.53	6	-	-	-	-	24	41
6b	0.53	6	3.6	0.110	0.85	~11 mm crease	-	-
7	0.54	10	(partial fail.)	-	-	-	-	-
			8.6	0.110	-	~4.5 mm crease	-	-
			(complete fail.)	-	-	-	-	-
7a	0.54	6	-	-	-	-	>19	-
8	0.54	10	11.8	0.036	0.73	~5 mm crease	-	-
8a	0.54	10	-	-	-	-	19	28
9	0.52	6	11.6	0.048	1.08	-	-	-
10	0.53	6	8.0	0.044	0.88	Narrow crease	27	40
11	0.51	6	2.6	-	-	-	-	-
11a	0.51	6	-	-	-	-	20	~40

Table V
SAND-SURROUNDED TUBE TESTS - CORRELATION BY "ARCHING THEORY"

Test No.	Soil Thickness (inches)	Initial Void Ratio	\bar{p}_o	u	\bar{p}_o/\bar{p}_i (ϕ)	\bar{p}_i	p_i tot = $\bar{p}_i + u$
17	0.188	0.545	4.65	-	2.07 (39°)	2.24	2.24
18			4.40	-		2.12	2.12
19			1.39	2.14		0.67	2.81
20			7.64	-		3.69	3.69
22	0.375	0.53	9.25	-	3.75 (39.5°)	2.47	2.47
24			5.50	1.20		1.47	2.67
26			1.00	2.60		0.27	2.87
N2	0.188	0.575	5.47	-	2.02 (38.4°)	2.71	2.71
N3			9.6	-		4.75	4.75
N5			1.45	1.71		0.72	2.43
N7			3.81	0.47		1.89	2.36
N23	0.375	0.60	9.70	-	3.45 (38°)	2.81	2.81
N25			4.87	0.77		1.41	2.18
N26			0.78	2.20		0.23	2.43

Theoretical buckling mode with $p_i = 2.5$ psi: $n = 15$, for unsupported buckling.

Table VI
 SAND-SURROUNDED TUBE TESTS -
 CORRELATION BY "ELASTIC BUCKLING" THEORY

Test No.	Thickness (inches)	Initial Void Ratio	\bar{p}_0	u	\bar{p}_i/\bar{p}_0	\bar{p}_i	$p_i \text{ tot} = \bar{p}_i + u$	k (psi/in)	n
17	0.188	0.545	4.65	-	1.09	5.06	5.06	690	14.8
18			4.40	-		4.80	4.80	620	14.5
19			1.39	2.14		1.52	3.66	360	12.6
20			7.64	-		8.33	8.33	1860	19.0
22	0.375	0.53	9.25	-	1.15	10.63	10.63	3040	21.5
24			5.50	1.20		6.32	7.52	1520	18.1
26			1.00	2.60		1.15	3.75	380	12.8
N2	0.188	0.575	5.47	-	1.09	5.96	5.96	950	16.1
N3			9.6	-		11.05	11.05	3280	22.0
N5			1.45	1.71		1.58	3.29	290	12.0
N7			3.81	0.47		4.15	4.62	570	14.2
N23	0.375	0.60	9.7	-	1.15	11.15	11.15	3340	22.0
N25			4.87	0.77		5.60	6.37	1090	16.6
N26			0.78	2.20		0.90	3.10	260	11.6

Table VII
GROUT-SURROUNDED TUBE TESTS - CORRELATIONS

Wall Thickness	Sample # AM-9	Observed		Predicted by Over-all Buckling Th.		Backcalculated from Elasting Buckling Th.	
		PCr (psi)	n	PCr (psi)	n	k (psi/in)	n
3/16"	9	0.59	5	0.56	4.5		
	18	1.32	3.8	1.12	4.0		
3/8"	9	0.81	5	1.6	3.8	17.7	6.0
	18	1.95	4.5	4.5	3.2	102	9.2

Table VIII

GROUT-SAND-SURROUNDED TUBES
CORRELATION BY "ELASTIC BUCKLING" THEORY

Test No.	Pcr =(pi) ² E (psi)	"Elastic Buckling" Theory		Observed n
		k (psi/in)	n	
3	2.0	107	9	-
4	2.7	195	11	12
5	2.0	107	9	13
6	1.7	78	9	11
6a	9.0	2180	20	~ 20
7	3.6	350	13	12
7	8.6	1980	19	29
8	11.8	3750	23	26
9	11.6	3620	22	-
10	8.0	1720	19	~ 20
11	2.6	181	11	-

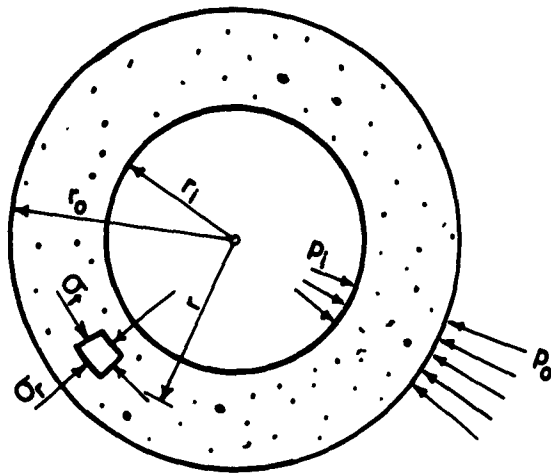


FIGURE 1 EQUILIBRIUM OF SOIL RING

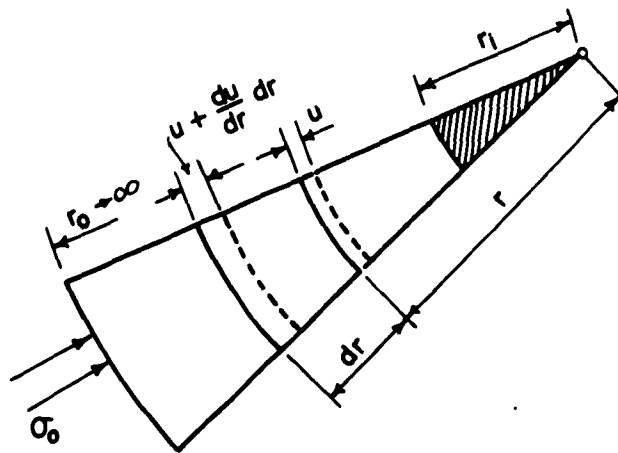
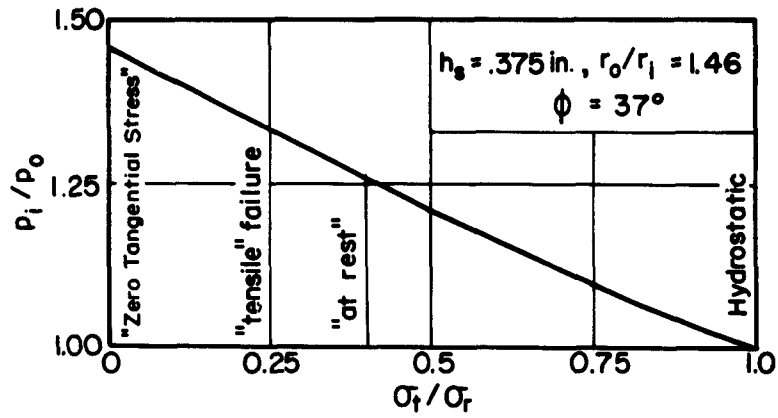
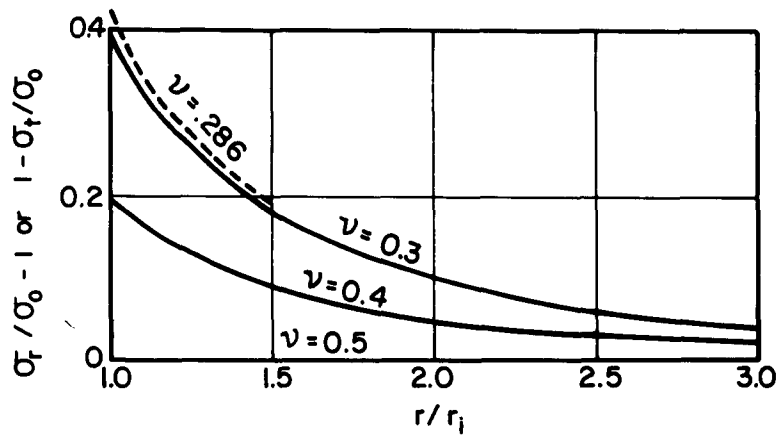


FIGURE 2 SOIL AROUND RIGID INCLUSION - PROBLEM

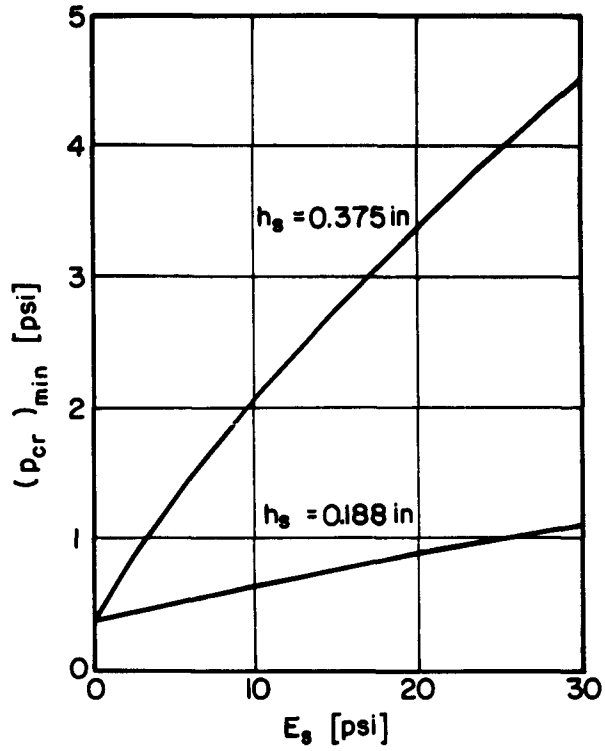


(a) p_i/p_o versus σ_t/σ_r (constant throughout the ring)

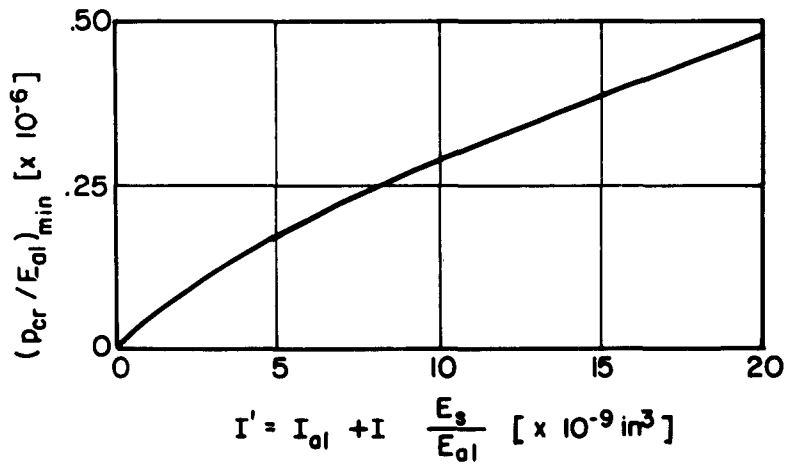


(b) Exact solution for rigid inclusion

FIGURE 3 SOIL AROUND RIGID INCLUSION - SOLUTIONS



(a) $(p_{cr})_{min}$ versus E_s



(b) $(p_{cr}/E_{al})_{min}$ versus I'

FIGURE 4 OVER-ALL BUCKLING OF COMPOSITE SAMPLE
Soil Surrounding 2-ply Aluminum Foil Tube

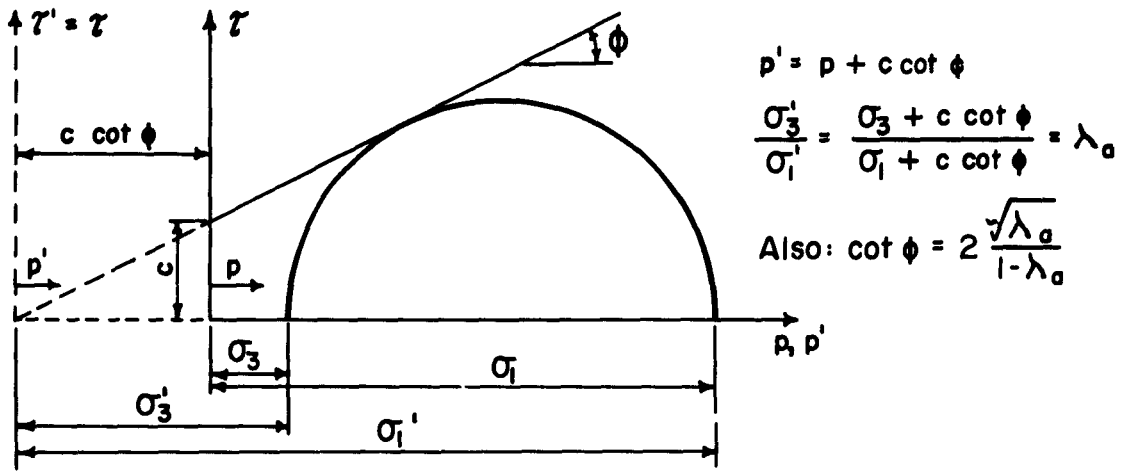


FIGURE 5 MOHR DIAGRAM FOR COHESIVE SOILS

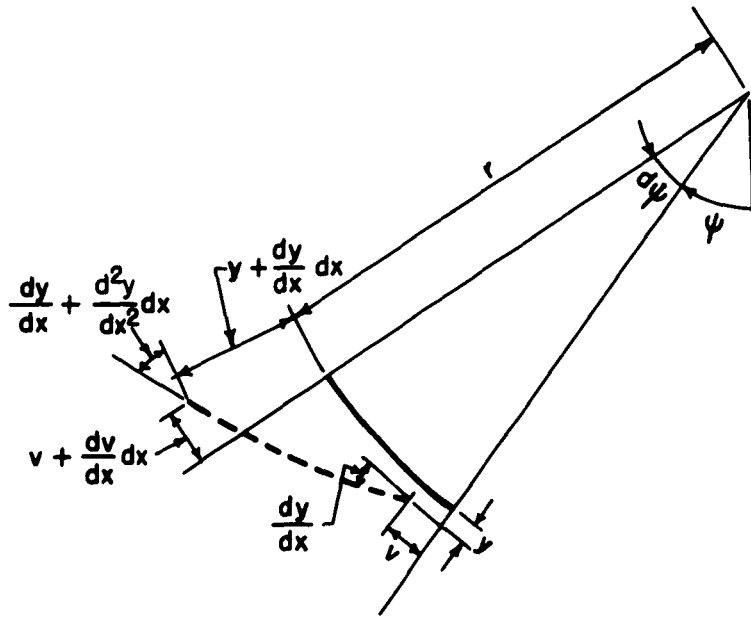


FIGURE 6 BUCKLING OF ELASTICALLY SUPPORTED RING

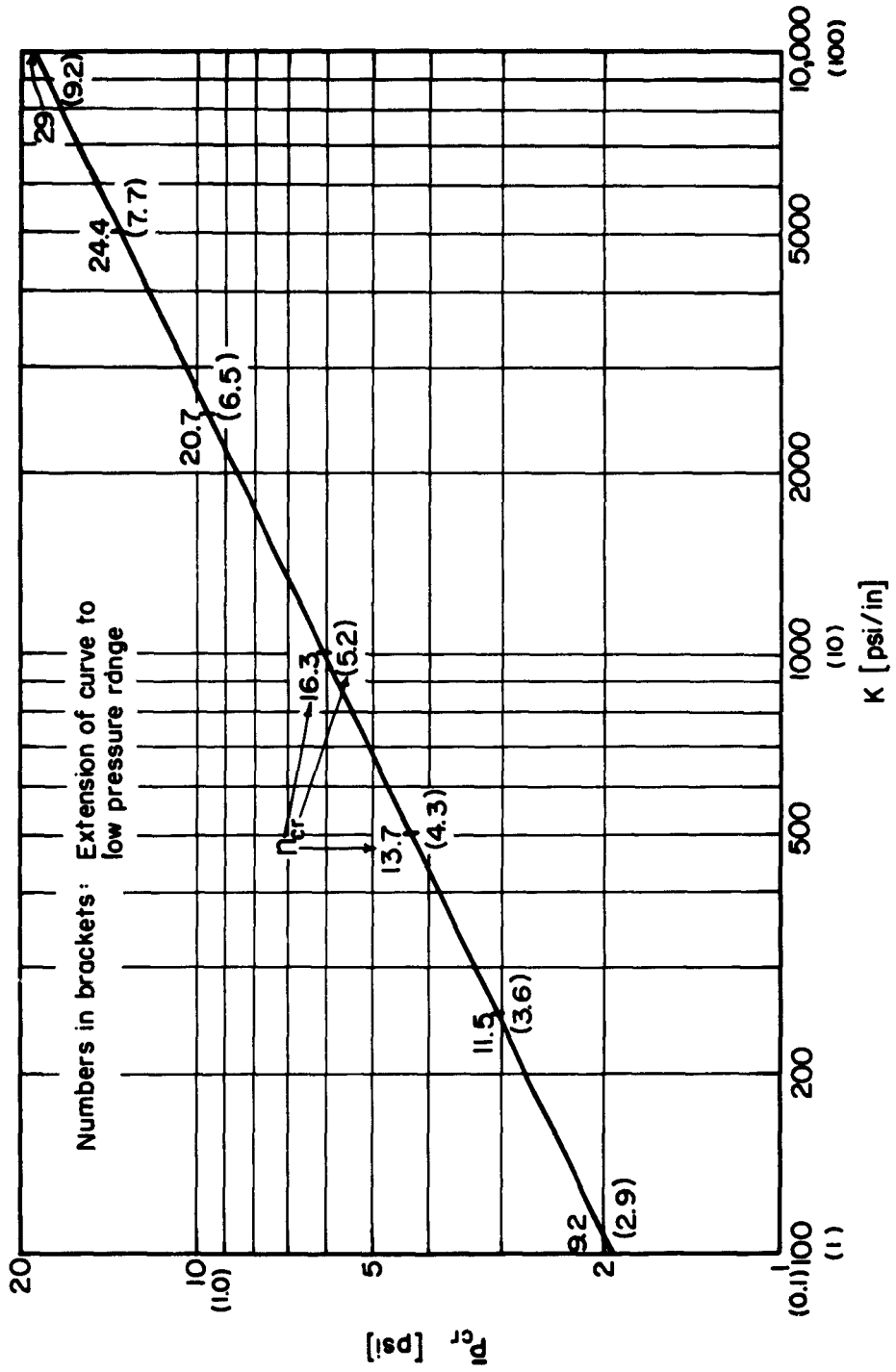
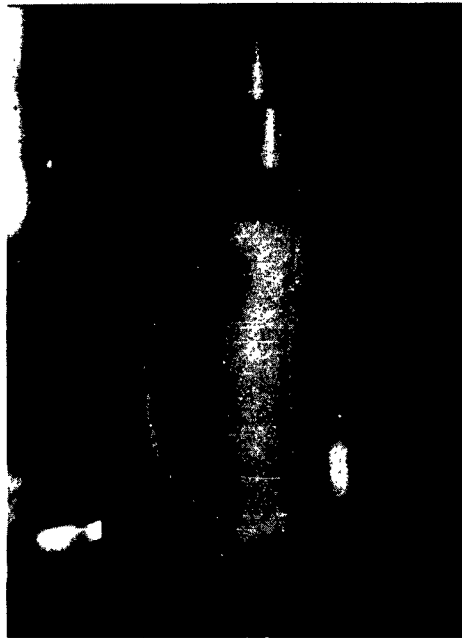
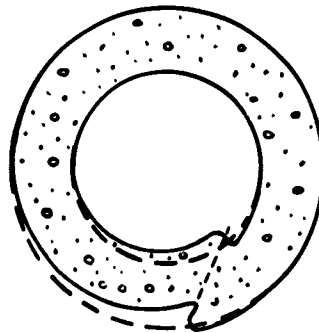


FIGURE 7 BUCKLING OF ELASTICALLY SUPPORTED RING - RESULTS



(a) Failed sample of 1in. I.D., 2 in. O.D.

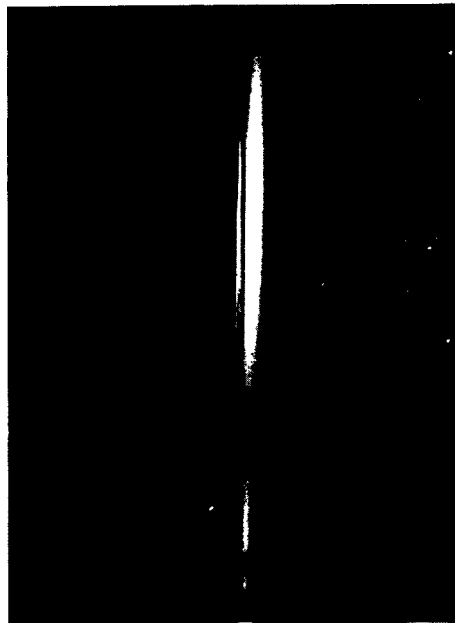


(b) Hypothesized cross section through a failed sample

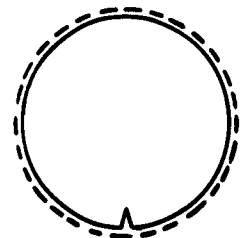
FIGURE 8 HOLLOW CYLINDER TESTS ON SAND



(a) Failed sample with 3/8 inch wall thickness
Large deformations

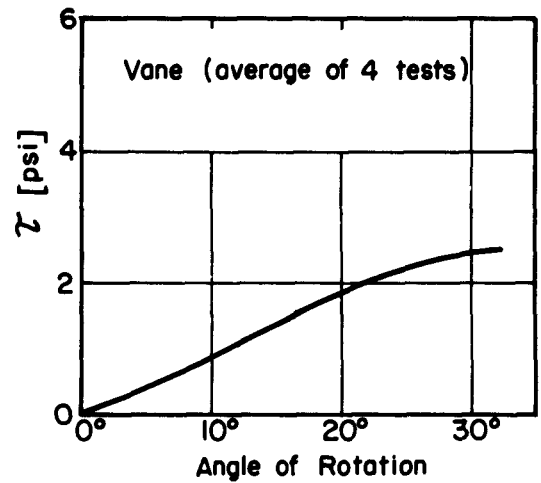
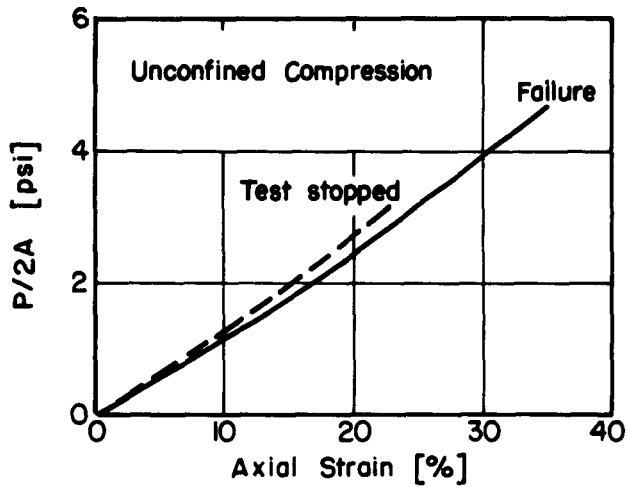


(b) Aluminum tube after failure
(3/8 inch soil thickness)
Only small deformations allowed

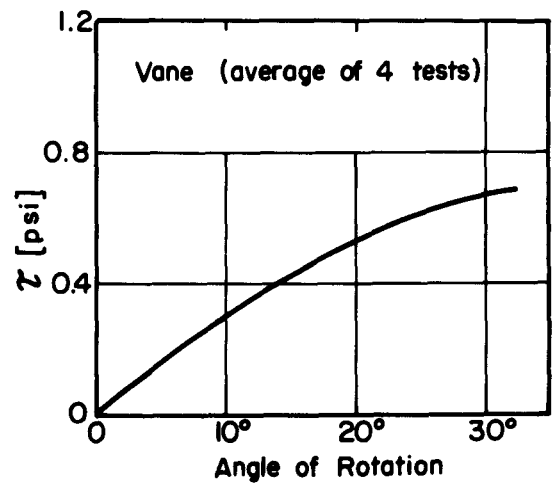
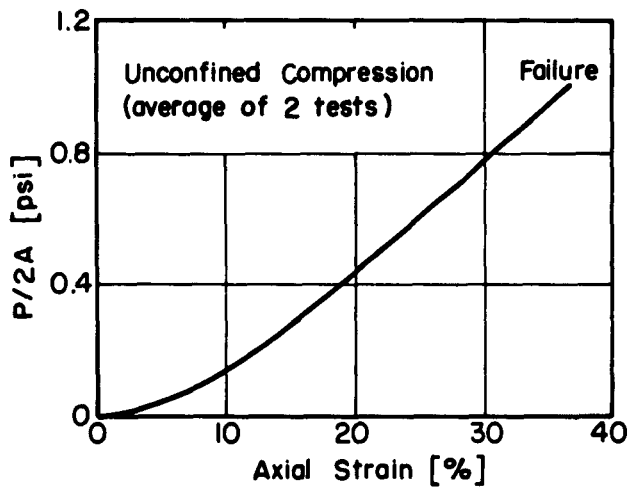


Cross Section

FIGURE 9 FAILURE PHENOMENA OF SAND-SURROUNDED TUBES

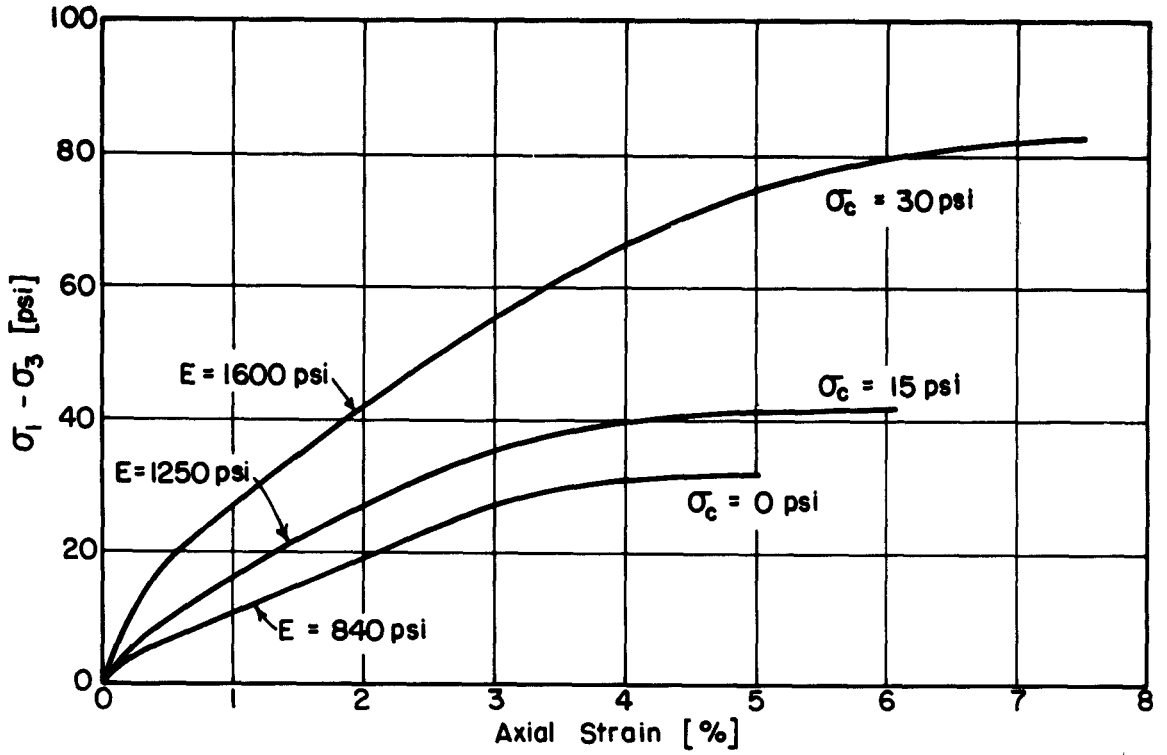


(a) 18% AM-9

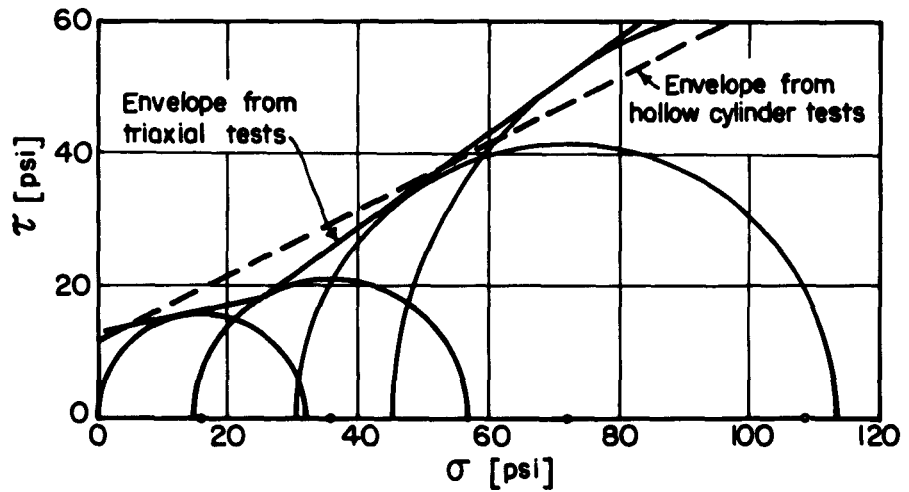


(b) 9% AM-9

FIGURE 10 PROPERTIES OF AM-9 GROUT



(a) Stress- Strain Curves

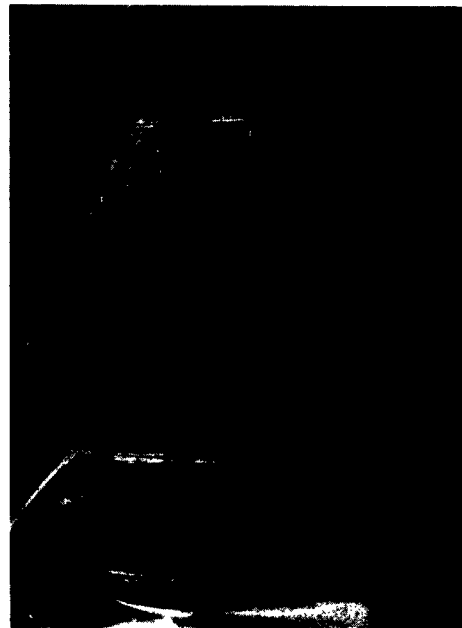


(b) Mohr diagram

FIGURE II TRIAXIAL TEST ON GROUT - SAND



a. View of failed cylinder



b. Cross section through failed cylinder

FIGURE 12 HOLLOW CYLINDER TESTS ON GROUT-SAND

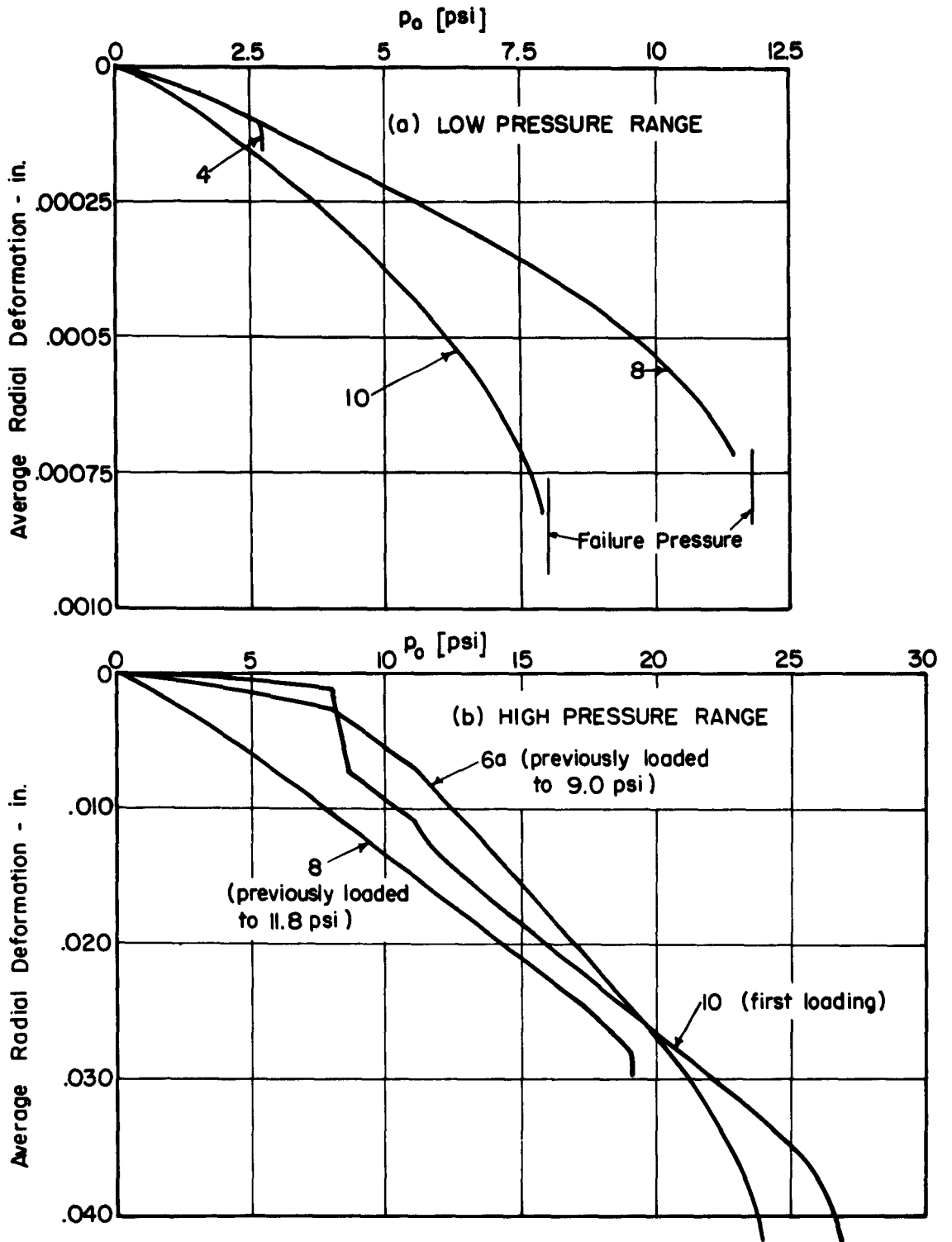


FIGURE 13 DEFORMATIONS OF GROUT-SAND-SURROUNDED TUBES

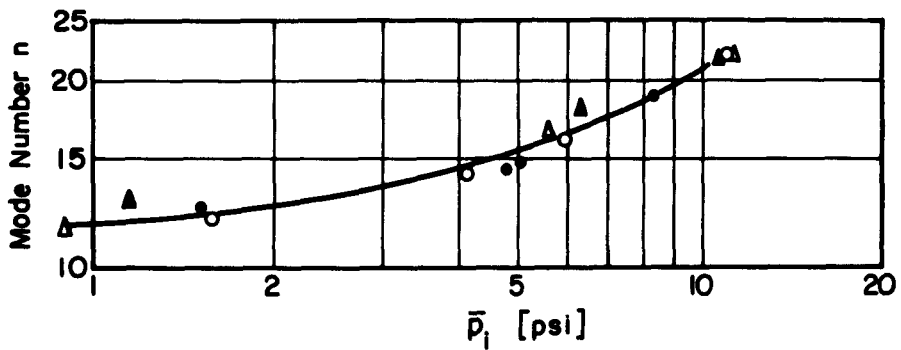
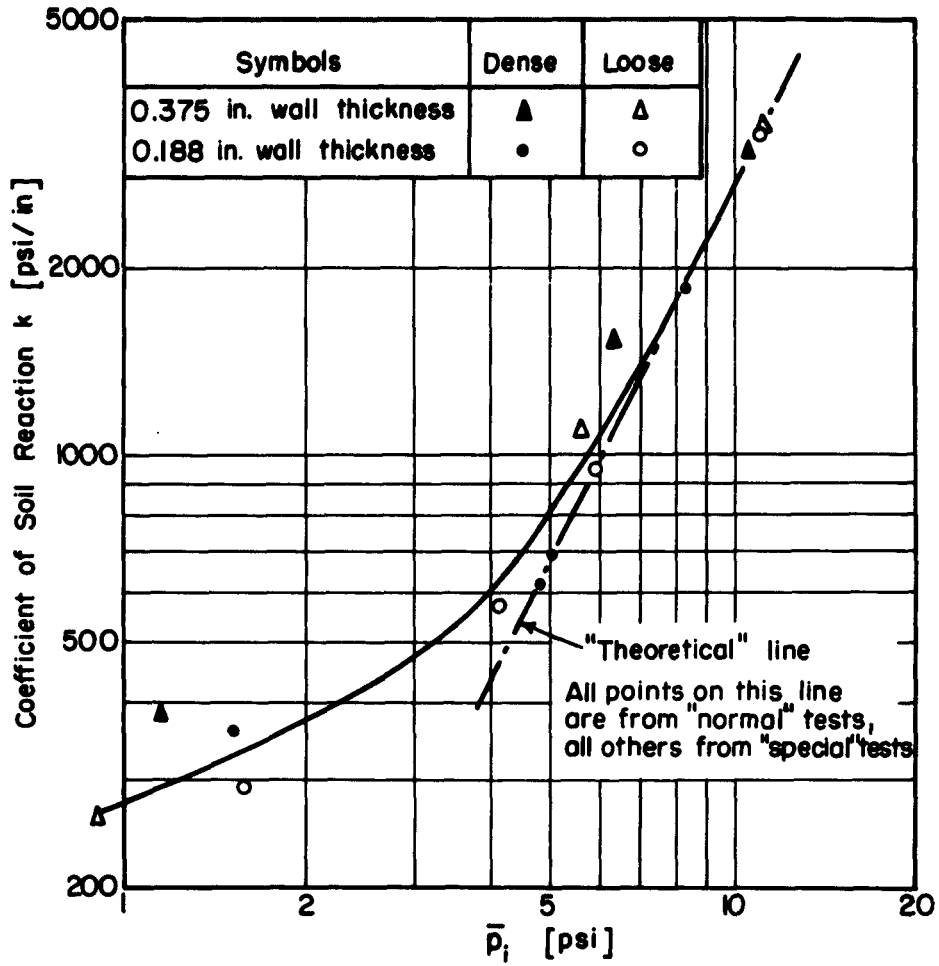


FIGURE 14 SAND-SURROUNDED TUBES
 Correlation by "Elastic Buckling" Theory

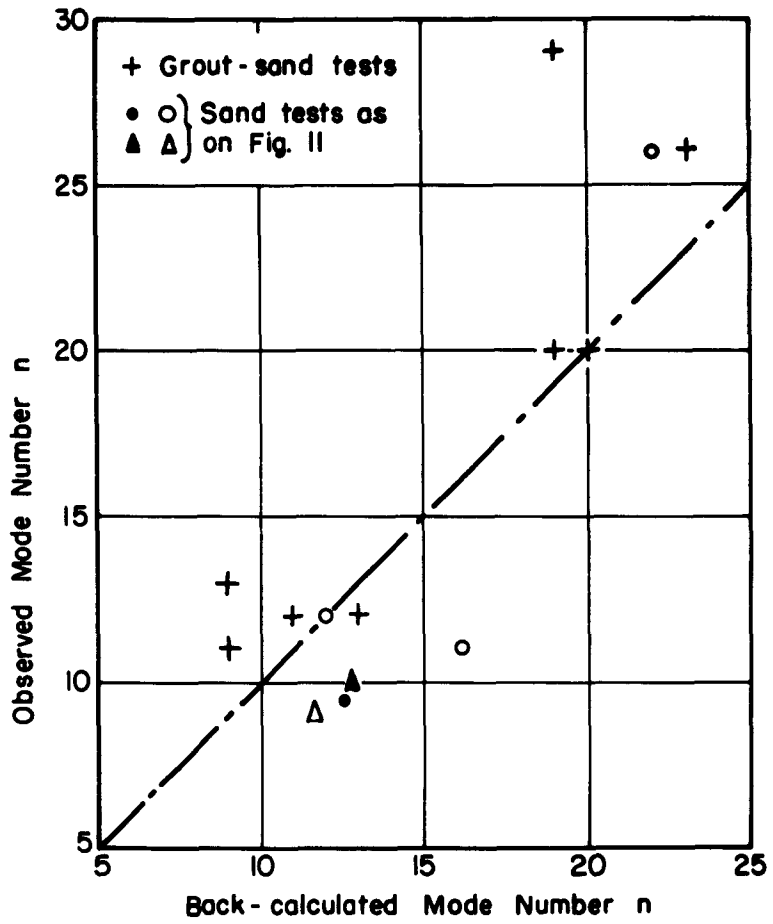
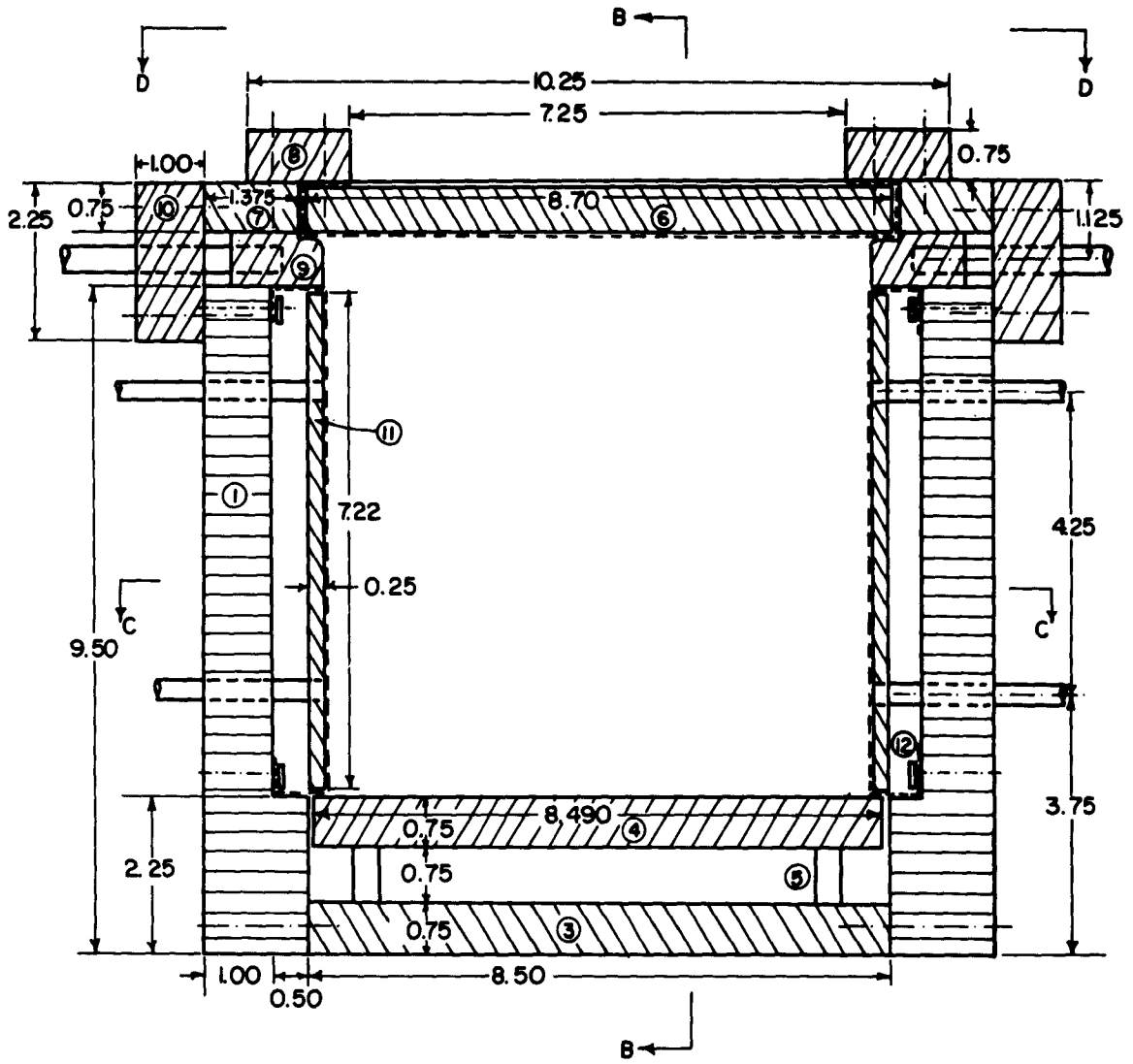


FIGURE 15 CORRELATION OF MODE NUMBERS

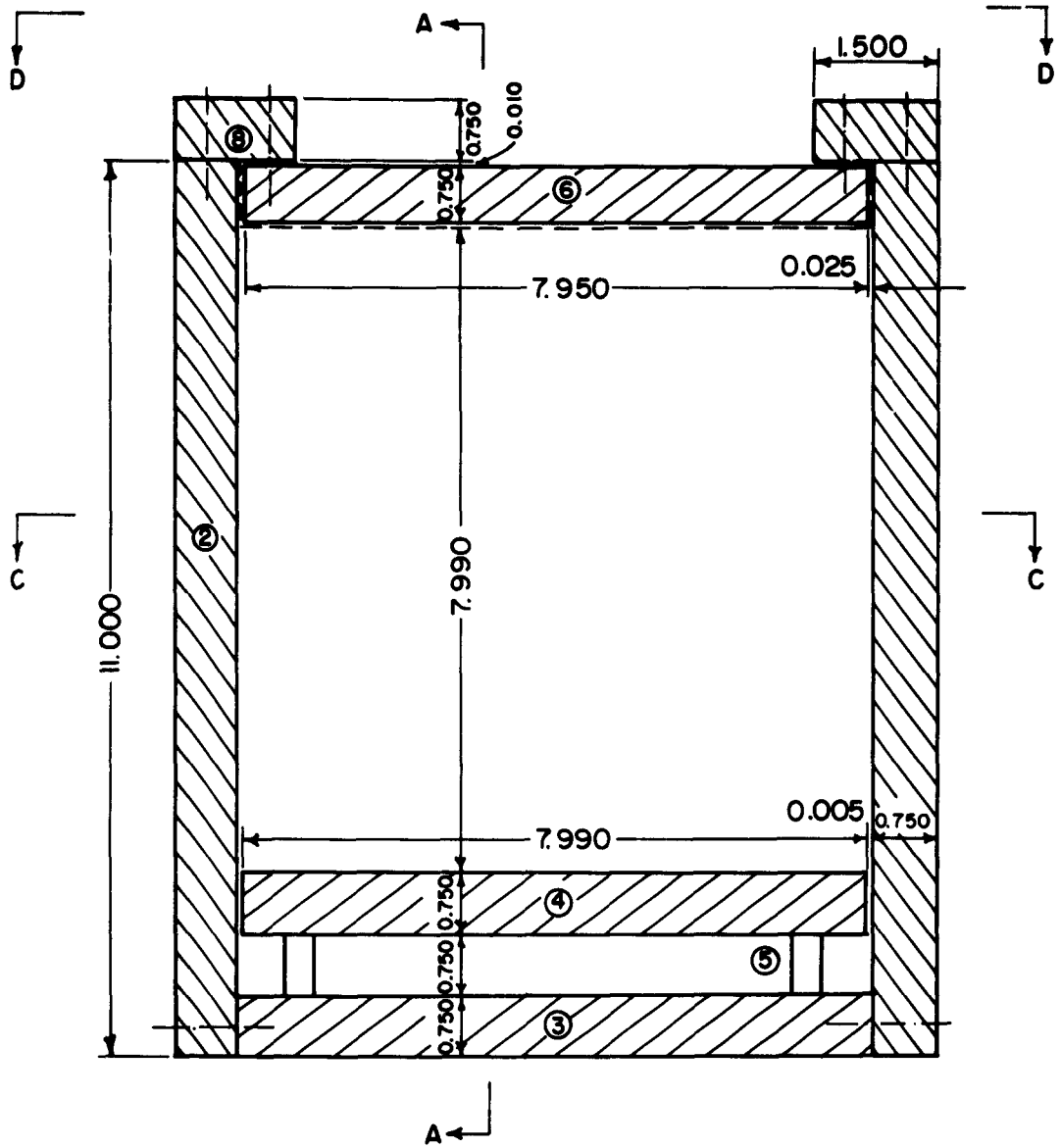
Other sections see Figs. 13 B, C, D
 List of components see Fig. 13 E



VERTICAL SECTION A-A

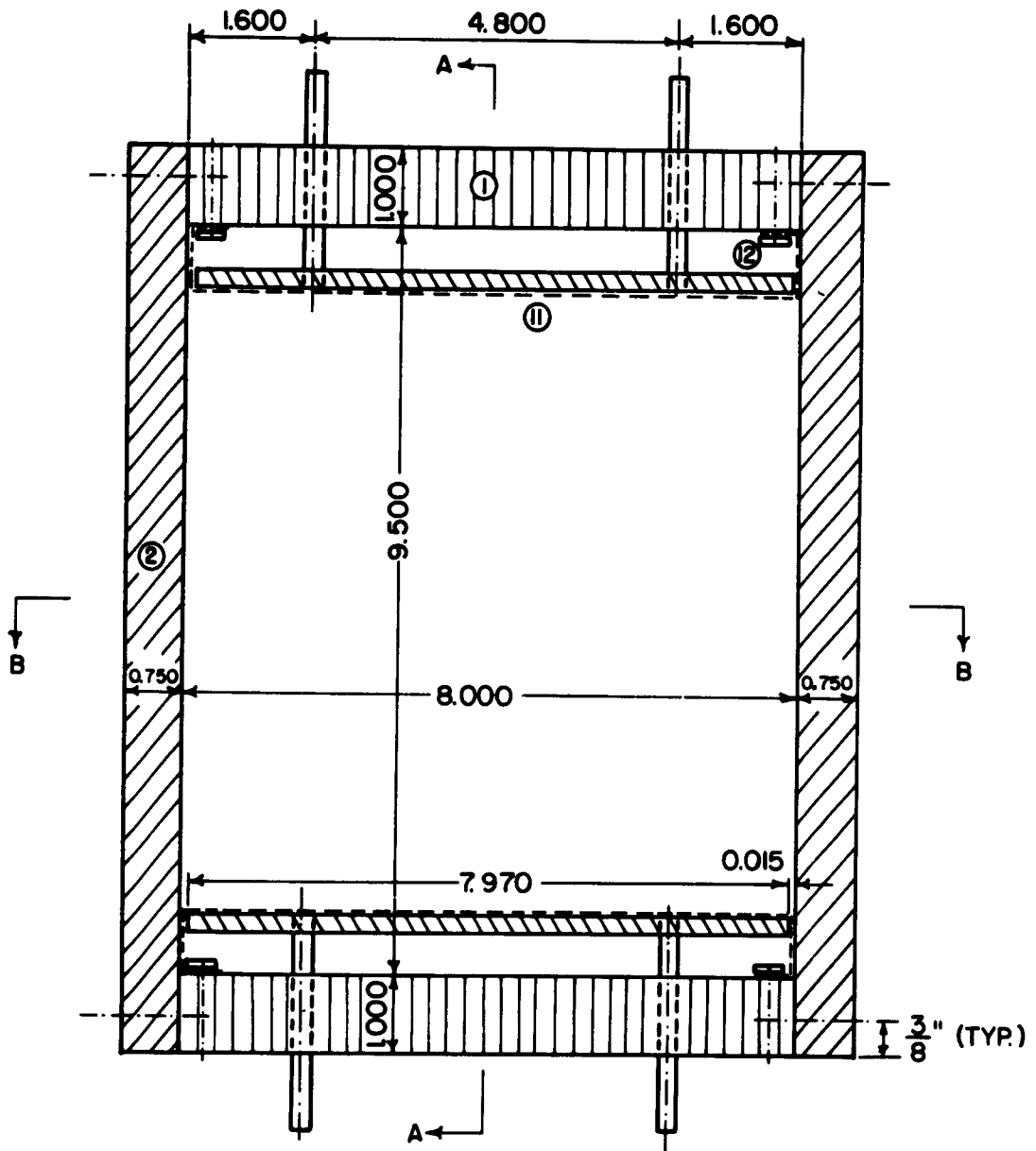
Scale $\frac{1}{2}$ " = 1"

FIGURE 16 A DRAWINGS OF PLANE STRAIN APPARATUS



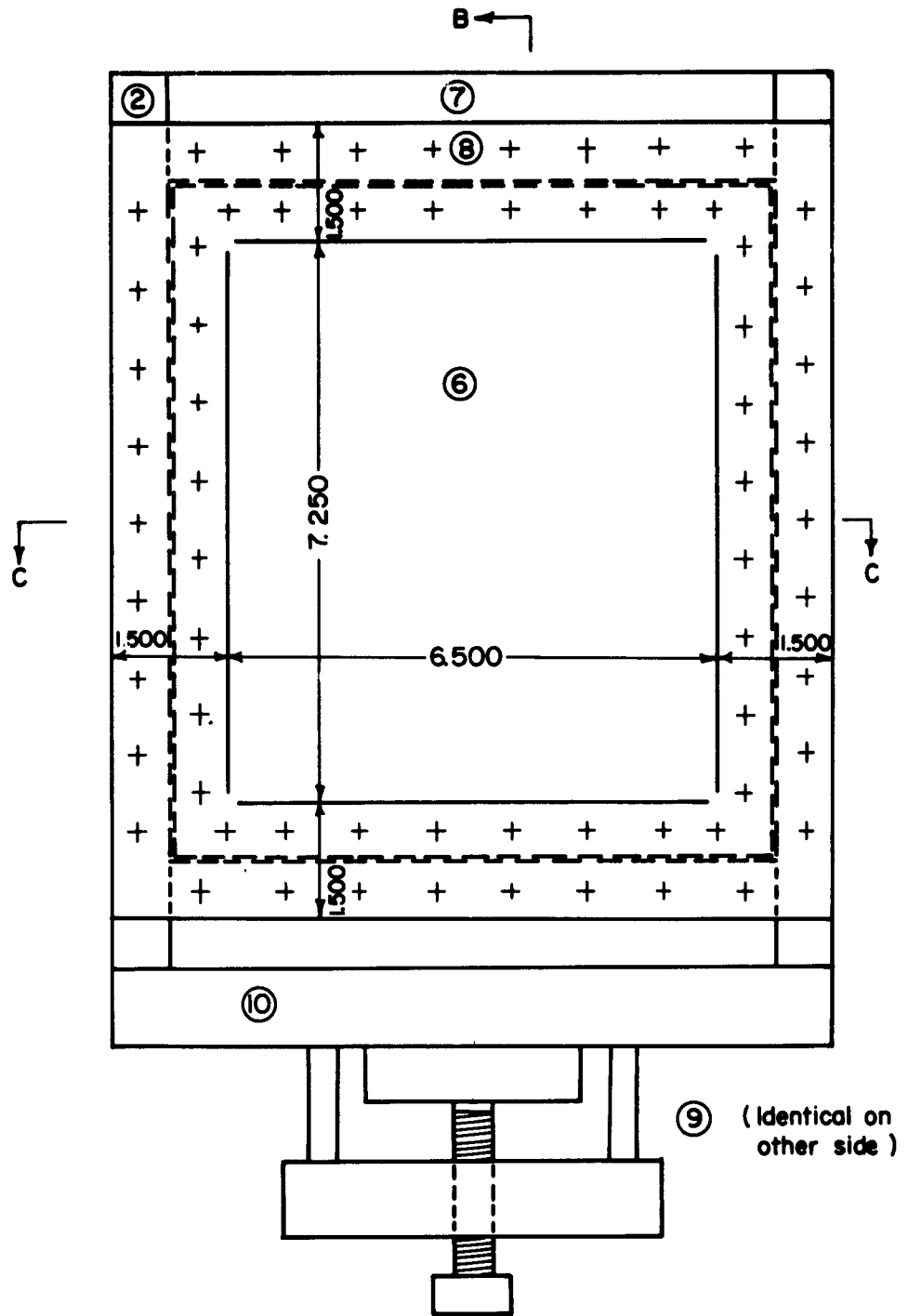
VERTICAL SECTION B-B

FIGURE 16 B DRAWINGS OF PLANE STRAIN APPARATUS



HORIZONTAL SECTION C-C

FIGURE 16 C DRAWINGS OF PLANE STRAIN APPARATUS



TOP VIEW D - D

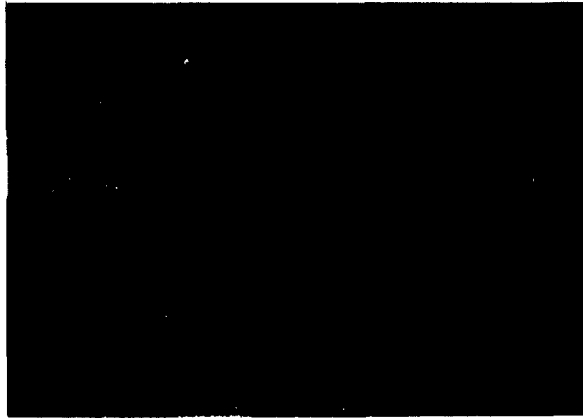
FIGURE 16D DRAWINGS OF PLANE STRAIN APPARATUS

LIST OF MAIN COMPONENTS

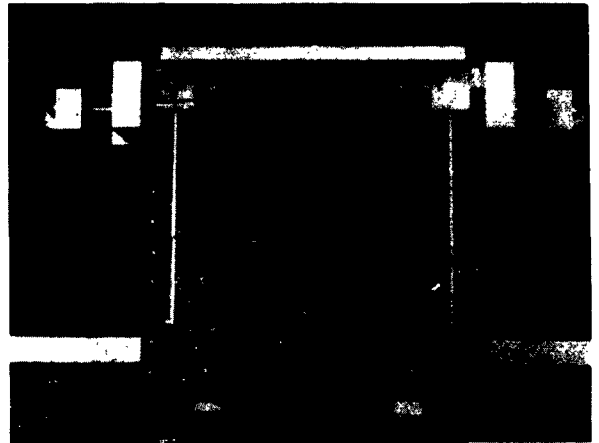
(All pieces of aluminum except as marked)

- ① Side plates (2) - Lucite
 - ② End plates (2)
 - ③ Bottom plate - Stainless steel
 - ④ Load plate - Stainless steel
 - ⑤ Load cell columns (4) - Stainless steel
 - ⑥ Top plate
 - ⑦ Top spacers (2)
 - ⑧ Top plate support
 - ⑨ Slider assemblies (2)
 - ⑩ Slider bushing supports (2)
 - ⑪ Membrane supporting assemblies (2) - Lucite
 - ⑫ Membrane sealing bands
- Membrane (3)
- + Bolts

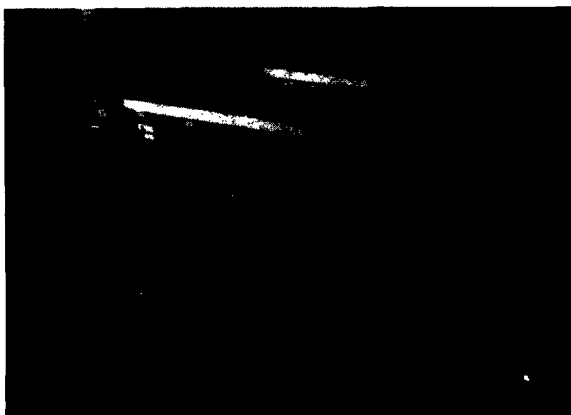
FIGURE 16 E DRAWINGS OF PLANE STRAIN APPARATUS



One end and
top removed



End removed



End removed

FIGURE 17 PHOTOS OF PLANE STRAIN APPARATUS

APPENDIX A

Appendix A

STRESSES AROUND A RIGID CIRCULAR INCLUSION

A plane strain solution for the case of a rigid circular inclusion in a uniformly stressed plane is presented here. Figure 2 of the main body has illustrated the problem and given the notation. The problem is point symmetrical; radial and tangential stresses are therefore principal stresses.

Radial direction: strain $\epsilon_r = \frac{du}{dr}$

Tangential direction: strain $\epsilon_t = \frac{u}{r}$

Axial direction: strain $\epsilon_a = 0$

Stress-strain relationships:

$$\epsilon_a = \frac{1}{E_s} [\sigma_a - \nu(\sigma_r + \sigma_t)] = 0$$

$$\sigma_a = \nu(\sigma_r + \sigma_t)$$

$$\epsilon_r = \frac{du}{dr} = \frac{1}{E_s} [\sigma_r - \nu(\sigma_t + \sigma_a)] = \frac{1}{E_s} [\sigma_r(1-\nu^2) - \sigma_t \nu(1+\nu)]$$

$$\epsilon_t = \frac{u}{r} = \frac{1}{E_s} [\sigma_t - \nu(\sigma_r + \sigma_a)] = \frac{1}{E_s} [\sigma_t(1-\nu^2) - \sigma_r \nu(1+\nu)]$$

$$\frac{du}{dr} \nu(1+\nu) + \frac{u}{r} (1-\nu^2) = \frac{\sigma_t}{E_s} [(1-\nu^2)^2 - \nu^2(1+\nu)^2]$$

$$\sigma_t = E_s \frac{u' \nu(1+\nu) + \frac{u}{r} (1-\nu^2)}{(1-\nu^2)^2 - \nu^2(1+\nu)^2} \quad \left(u' = \frac{du}{dr} \right)$$

$$\frac{du}{dr} (1-\nu^2) + \frac{u}{r} \nu(1+\nu) = \frac{\sigma_r}{E_s} [(1-\nu^2)^2 - \nu^2(1+\nu)^2]$$

$$\sigma_r = E_s \frac{u' (1-\nu^2) + \frac{u}{r} \nu(1+\nu)}{(1-\nu^2)^2 - \nu^2(1+\nu)^2}$$

After simplification

$$\bar{\sigma}_t = \frac{E_s}{(1+\nu)(1-2\nu)} [u'v + u'_r (1-\nu)]$$

$$\bar{\sigma}_r = \frac{E_s}{(1+\nu)(1-2\nu)} [u'(1-\nu) + u'_r \nu]$$

Also:
$$\frac{d\bar{\sigma}_r}{dr} = \frac{E_s}{(1+\nu)(1-2\nu)} [u''(1-\nu) + u''_r \nu - \frac{u'_r}{r^2} \nu]$$

Equilibrium equation:
$$\frac{d\bar{\sigma}_r}{dr} r + \bar{\sigma}_r - \bar{\sigma}_t = 0 \quad (1)$$

After substitution and simplification:

$$r^2 u'' + r u' - u = 0 \quad (6)$$

By substituting $u = r^x$, the general solution of (6) is obtained as

$$u = C_1 r + C_2 r$$

Boundary conditions:

At inner boundary ($r = r_i$): $u(r_i) = 0$

$$c_1 + c_2 r_i^2 = 0$$

At outer boundary ($r \rightarrow \infty$): displacements of uniform stress field:

$$u(r_o) = \frac{r_o}{E_s} \bar{\sigma}_o [(1-\nu^2) - \nu(1+\nu)]$$

$$u(r_o) = \frac{r_o}{E_s} \bar{\sigma}_o (1-\nu-2\nu^2)$$

Thus:

$$C_2 r_o = \frac{r_o}{E_s} \bar{\sigma}_o (1 - \nu - 2\nu^2)$$

$$C_2 = \frac{\bar{\sigma}_o}{E_s} (1 - \nu - 2\nu^2)$$

$$C_1 = -C_2 r_i^2 = -\frac{r_i^2 \bar{\sigma}_o}{E_s} (1 - \nu - 2\nu^2)$$

Substituted:

$$u = r \frac{\bar{\sigma}_o}{E_s} (1 - \nu - 2\nu^2) \left[1 - \left(\frac{r_i}{r} \right)^2 \right] \quad (7)$$

$$\frac{du}{dr} = \frac{\bar{\sigma}_o}{E_s} (1 - \nu - 2\nu^2) \left[1 + \left(\frac{r_i}{r} \right)^2 \right]$$

Then:

$$\sigma_r = \bar{\sigma}_o \left[1 + \left(\frac{r_i}{r} \right)^2 (1 - 2\nu) \right] \quad (8)$$

$$\sigma_t = \bar{\sigma}_o \left[1 - \left(\frac{r_i}{r} \right)^2 (1 - 2\nu) \right]$$

Plots of these expressions, for $\nu = 0.4, 0.3$ and 0.280 , are presented in Figure 3b of the main body.

APPENDIX B

Appendix B

BUCKLING OF AN ELASTICALLY SUPPORTED RING

A solution for buckling of an elastically supported ring is presented here. Figure 6 of the main body illustrates the problem and clarifies the notation. The solution is quite similar to Hetenyi's (Ref. (6)), but here the equilibrium equations are formulated for the deformed shape rather than the original shape of the ring. Another reference which was used for the present derivation was Timoshenko (Ref. (5)).

$$\text{Applied pressure: } p = \bar{p} + ky$$

Equilibrium equations:

$$\text{Radial direction: } p dx' - N d\psi' = dQ$$

$$\text{where } dx' = dx + \Delta dx = dx \left(1 - \frac{N}{AE}\right)$$

$$d\psi' = d\psi + \Delta d\psi = d\psi - \frac{d^2 y}{dx^2} dx$$

$$dx = r d\psi \quad \text{or} \quad \frac{d}{dx} = \frac{1}{r} \frac{d}{d\psi}$$

and N = normal force in ring

Q = shear force in ring

A = area of ring

$$\text{then: } p \left(1 - \frac{N}{AE}\right) - \frac{N}{r} + N \frac{d^2 y}{dx^2} = \frac{dQ}{dx}$$

Tangential direction:

$$Q d\psi' = dN$$

$$Q d\psi - Q \frac{d^2 y}{dx^2} dx = dN$$

$$Q/r - Q \frac{d^2 y}{dx^2} = \frac{dN}{dx}$$

moments: $dM = Q dx' = Q dx (1 - N/AE)$

where M = bending moment in ring

then: $Q (1 - N/AE) = \frac{dM}{dx}$

A number of simplifications are introduced at this point:

(a) In the corrective terms (those which represent the consideration of deformations), forces and moments are replaced by those which would be present in the unbuckled ring; that is, in these terms, $N = N_0 = r\bar{p}$, $Q = Q_0 = 0$, $M = M_0 = 0$. This step corresponds to a neglecting of corrective terms of second order, which is a common procedure in problems of this kind.

(b) The term N_0/AE is very small compared to 1.

Thus $1 - N_0/AE = 1$.

With these simplifications, the equilibrium equations are:

$$\bar{p} + ky - \frac{N}{r} + N \frac{d^2 y}{dx^2} = \frac{dQ}{dx}$$

$$Q/r = \frac{dN}{dx}$$

$$Q = \frac{dM}{dx}$$

Eliminating Q and N, the following equation is obtained:

$$k \frac{dy}{dx} - \frac{1}{r^2} \frac{dM}{dx} + \bar{p} r \frac{d^2 y}{dx^2} = \frac{d^3 M}{dx^3} \quad (B1)$$

The differential equation of bending of a circular arc is, according to Hetenyi and Timoshenko:

$$\frac{d^2y}{dx^2} + \frac{y}{r^2} = - \frac{M}{EI} \quad (B2)$$

If this equation and its third derivative are substituted in (B1) to eliminate M, one obtains, after substituting $d/dx = \frac{1}{r} \frac{d}{d\psi}$:

$$\frac{d^5y}{d\psi^5} + \frac{d^3y}{d\psi^3} (2 + \bar{p}a) + \frac{dy}{d\psi} (kra + 1) = 0 \quad (12)$$

$$\text{where } a = \frac{r^3}{EI}$$

Exploring the possibility of a periodic buckled shape, $y = B \sin n\psi$ is substituted into Equation (12). The result is:

$$n^5 - n^3 (2 + \bar{p}a) + n (kra + 1) = 0 \quad (13)$$

Excluding from consideration the solution $n = 0$ yields:

$$n^4 - n^2 (2 + \bar{p}a) + kra + 1 = 0$$

This equation can be further treated by formulating a solution for n^2 , then finding the smallest \bar{p} for which n has a real solution. Alternatively, the equation can be solved for \bar{p} and minimized with respect to n . By either method of solution, the result is:

$$\bar{p}_{cr} = \frac{2}{a} (\sqrt{kra + 1} - 1) \quad (B3)$$

$$n_{cr} = \sqrt[4]{kra + 1} \quad (B4)$$

For the 2-ply aluminum tube used in this work,

$$a = r^3/EI = 87 \text{ in}^2/\text{lb}, \text{ and } r = 0.812 \text{ inch.}$$

Thus, for $k \geq 10 \text{ psi/in.}$, which will always be the case, $l \ll kra$, and $l \ll \sqrt{kra}$.

Therefore:

$$\bar{p}_{cr} = 2\sqrt{\frac{kr}{a}} \quad (14)$$

$$n_{cr} = \sqrt[4]{kra} \quad (15)$$

Since it is stated in Reference (6) that Equation (B2) neglects rib shortening of the arch, a new differential equation of arch deformation considering rib shortening was derived:

$$\frac{d^2y}{dx^2} = -\frac{M}{EI} + \frac{N}{AER} \quad (B5)$$

When combined with $\frac{dN}{dx} = \frac{1}{r} \frac{dM}{dx}$ as derived earlier, the equation becomes

$$\frac{d^3y}{dx^3} = -\frac{1}{EI} \frac{dM}{dx} \quad (B6)$$

Substituting this equation in Equation (B1) and simplifying, a substitute differential equation for (12) is obtained:

$$\frac{d^5y}{dy^5} + \frac{d^3y}{dy^3} (1 + \bar{p}a) + \frac{dy}{dy} kra = 0 \quad (B7)$$

The final result is slightly different from Equations (B2) and (B3) only in the terms which were subsequently neglected, and the result in the form of Equations (14) and (15) is unchanged.

DISTRIBUTION

No. cys

HEADQUARTERS USAF

2 Hq USAF (AFOCE), Wash 25, DC
 1 Hq USAF (AFRST), Wash 25, DC
 1 Hq USAF (AFRNE-A, Maj Lowry), Wash 25, DC
 1 Hq USAF (AFTAC), Wash 25, DC
 1 USAF Dep, The Inspector General (AFIDI), Norton AFB, Calif
 1 USAF Directorate of Nuclear Safety (AFINS), Kirtland AFB, NM
 1 AFOAR, Bldg T-D, Wash 25, DC

MAJOR AIR COMMANDS

1 AFSC (SCT), Andrews AFB, Wash 25, DC
 2 AUL, Maxwell AFB, Ala
 2 USAFIT (USAF Institute of Technology), Wright-Patterson AFB, Ohio

AFSC ORGANIZATIONS

1 AFSC Regional Office, 6331 Hollywood Blvd., Los Angeles 28, Calif
 1 ASD (ASAPRL, Technical Doc Library), Wright-Patterson AFB, Ohio
 3 BSD (BSR), Norton AFB, Calif
 3 SSD (SSSC-TDC), AF Unit Post Office, Los Angeles 45, Calif
 2 ESD (ESAT), Hanscom Fld, Bedford, Mass
 1 AF Msl Dev Cen (RRR-T), Holloman AFB, NM
 1 AFMTC (MU-135), Patrick AFB, Fla
 2 APGC (PGAPI), Eglin AFB, Fla
 2 AEDC (AEOI), Arnold Air Force Station, Tenn

KIRTLAND AFB ORGANIZATIONS

AFSWC, Kirtland AFB, NM
 1 (SWEH)
 30 (SWOI)
 5 (SWRS)
 1 US Naval Weapons Evaluation Facility (NWEF) (Code 404), Kirtland AFB, NM

DISTRIBUTION (cont'd)

No. cys

OTHER AIR FORCE AGENCIES

2 Director, USAF Project RAND, via: Air Force Liaison Office,
The RAND Corporation (RAND Library), 1700 Main Street,
Santa Monica, Calif

ARMY ACTIVITIES

2 Director, Ballistic Research Laboratories (Library), Aberdeen
Proving Ground, Md

1 Hq US Army Air Defense Command (ADGCB), Ent AFB, Colo

1 Chief of Engineers, Department of the Army (ENGEA), Wash 25,
DC

2 Office of the Chief, Corps of Engineers, US Army (Protective
Construction Branch), Wash 25, DC

1 Director, Army Research Office, Arlington Hall Sta, Arlington, Va

2 Director, US Army Waterways Experiment Sta (WESRL), P.O.
Box 60, Vicksburg, Miss

1 Commanding Officer, US Army Engineers, Research & Develop-
ment Laboratories, Ft Belvoir, Va

NAVY ACTIVITIES

1 Chief, Bureau of Yards and Docks, Department of the Navy,
Wash 25, DC

1 Chief, Bureau of Ships, Department of the Navy, Wash 25, DC

1 Commanding Officer and Director, David Taylor Model Basin,
Wash 7, DC

1 Commanding Officer and Director, Naval Civil Engineering
Laboratory, Port Hueneme, Calif

1 Commander, Naval Ordnance Test Station, Inyokern (Code 12),
China Lake, Calif

1 Officer-in-Charge, Civil Engineering Corps Officers, US Naval
School, Naval Construction Battalion Center, Port Hueneme, Calif

1 Office of Naval Research, Wash 25, DC

OTHER DOD ACTIVITIES

Chief, Defense Atomic Support Agency, Wash 25, DC

1 (Document Library)

2 (DASABS)

DISTRIBUTION (cont'd)

No. cys

- 2 Commander, Field Command, Defense Atomic Support Agency (FCAG3, Special Weapons Publication Distribution), Sandia Base, NM
- 1 Director, Advanced Research Projects Agency, Department of Defense, The Pentagon, Wash 25, DC
- 1 Director, Defense Research & Engineering, The Pentagon, Wash 25, DC
- 10 ASTIA (TIPDR), Arlington Hall Sta, Arlington 12, Va

AEC ACTIVITIES

- 1 Sandia Corporation (Tech Library), Sandia Base, NM
- 1 Sandia Corporation (Tech Library), P. O. Box 969, Livermore, Calif

OTHER

- 1 Office of Assistant Secretary of Defense (Civil Defense), Battle Creek, Mich
- 1 Space Technology Labs, Inc., ATTN: Information Center, Document Procurement, P. O. Box 95001, Los Angeles 45, Calif
- 2 University of Illinois, Talbot Laboratory, Room 207, Urbana, Ill
- 30 Massachusetts Institute of Technology, Department of Civil & Sanitary Engineering, ATTN: Prof. R. V. Whitman, 77 Massachusetts Avenue, Cambridge, Mass
- 2 South Dakota School of Mines and Technology, ATTN: Prof. Edwin H. Oshier, Rapid City, South Dakota
- 2 University of New Mexico, AF Shock Tube Facility, Box 188, University Station, Albuquerque, NM
- 2 Armour Research Foundation, ATTN: Dr. Sevin, 3422 South Dearborn St., Chicago 15, Ill
- 2 MRD Division, General American Transportation Corp., 7501 North Natchez Avenue, Niles 48, Ill
- 1 National Engineering Science Co., ATTN: Dr. Soldate, 711 South Fair Oaks Ave., Pasadena, Calif
- 1 The Dikewood Corporation, 4805 Menaul Blvd., N.E., Albuquerque, NM
- 1 United Research Services, 1811 Trousdale Drive, Burlingame, Calif
- 1 University of Notre Dame, Department of Civil Engineering, ATTN: Dr. H. Saxe, Notre Dame, Ind

TDR-63-6

DISTRIBUTION (cont'd)

No. cys

2	Stanford Research Institute, Menlo Park, Calif
1	Stanford University, School of Mechanical Engineering, ATTN: Dr. Jacobsen, Stanford, Calif
1	University of Washington, ATTN: Dr. I. M. Fyfe, Seattle 5, Wash
2	Purdue University, School of Civil Engineering, ATTN: Prof. G. A. Leonards, Lafayette, Ind
1	California Institute of Technology, ATTN: Dr. Paul Blatz, 1201 East California Blvd., Pasadena, Calif
1	Paul Weidlinger and Associates, 770 Lexington Avenue, New York 21, NY
1	Official Record Copy (SWRS)

<p>Air Force Special Weapons Center, Kirtland AF Base, New Mexico Rpt. No. AFSWC-TDR-63-6. STUDY OF THE COLLAPSE OF SMALL SOIL-SURROUNDED TUBES. Interim Report, March 1963. 82 p. incl illus., tables, 7 refs. Unclassified Report</p>	<p>1. Pressure 2. Soil mechanics 3. Stress and strain 4. Structural elements -- effects of blast</p> <p>I. AFSC Project 1080, Task 108001 II. Contract AF 29(601)-4927 III. Massachusetts Inst. of Tech., Cambridge, Dept. of Civil Engineering IV. Ulrich Luscher V. DASA WEB No. 13.145 VI. In ASTIA collection</p>	<p>Air Force Special Weapons Center, Kirtland AF Base, New Mexico Rpt. No. AFSWC-TDR-63-6. STUDY OF THE COLLAPSE OF SMALL SOIL-SURROUNDED TUBES. Interim Report, March 1963. 82 p. incl illus., tables, 7 refs. Unclassified Report</p>	<p>1. Pressure 2. Soil mechanics 3. Stress and strain 4. Structural elements -- effects of blast</p> <p>I. AFSC Project 1080, Task 108001 II. Contract AF 29(601)-4927 III. Massachusetts Inst. of Tech., Cambridge, Dept. of Civil Engineering IV. Ulrich Luscher V. DASA WEB No. 13.145 VI. In ASTIA collection</p>	<p>Air Force Special Weapons Center, Kirtland AF Base, New Mexico Rpt. No. AFSWC-TDR-63-6. STUDY OF THE COLLAPSE OF SMALL SOIL-SURROUNDED TUBES. Interim Report, March 1963. 82 p. incl illus., tables, 7 refs. Unclassified Report</p>	<p>This report describes a program of experimental and theoretical work on the problem of failure of structural tubes surrounded by a thin layer of soil loaded by uniform radial outside pressures. The properties and the thickness of the soil layer were varied, and the failure pressure of the tube, as well as the deformations of the tube before and after failure, was observed. Theories based on idealized models of the soil-structure interaction were developed. The experimental results were then correlated with these theories</p>	<p>This report describes a program of experimental and theoretical work on the problem of failure of structural tubes surrounded by a thin layer of soil loaded by uniform radial outside pressures. The properties and the thickness of the soil layer were varied, and the failure pressure of the tube, as well as the deformations of the tube before and after failure, was observed. Theories based on idealized models of the soil-structure interaction were developed. The experimental results were then correlated with these theories</p>	<p>This report describes a program of experimental and theoretical work on the problem of failure of structural tubes surrounded by a thin layer of soil loaded by uniform radial outside pressures. The properties and the thickness of the soil layer were varied, and the failure pressure of the tube, as well as the deformations of the tube before and after failure, was observed. Theories based on idealized models of the soil-structure interaction were developed. The experimental results were then correlated with these theories</p>	<p>This report describes a program of experimental and theoretical work on the problem of failure of structural tubes surrounded by a thin layer of soil loaded by uniform radial outside pressures. The properties and the thickness of the soil layer were varied, and the failure pressure of the tube, as well as the deformations of the tube before and after failure, was observed. Theories based on idealized models of the soil-structure interaction were developed. The experimental results were then correlated with these theories</p>	<p>This report describes a program of experimental and theoretical work on the problem of failure of structural tubes surrounded by a thin layer of soil loaded by uniform radial outside pressures. The properties and the thickness of the soil layer were varied, and the failure pressure of the tube, as well as the deformations of the tube before and after failure, was observed. Theories based on idealized models of the soil-structure interaction were developed. The experimental results were then correlated with these theories</p>
<p>1. Pressure 2. Soil mechanics 3. Stress and strain 4. Structural elements -- effects of blast</p> <p>I. AFSC Project 1080, Task 108001 II. Contract AF 29(601)-4927 III. Massachusetts Inst. of Tech., Cambridge, Dept. of Civil Engineering IV. Ulrich Luscher V. DASA WEB No. 13.145 VI. In ASTIA collection</p>	<p>Air Force Special Weapons Center, Kirtland AF Base, New Mexico Rpt. No. AFSWC-TDR-63-6. STUDY OF THE COLLAPSE OF SMALL SOIL-SURROUNDED TUBES. Interim Report, March 1963. 82 p. incl illus., tables, 7 refs. Unclassified Report</p>	<p>1. Pressure 2. Soil mechanics 3. Stress and strain 4. Structural elements -- effects of blast</p> <p>I. AFSC Project 1080, Task 108001 II. Contract AF 29(601)-4927 III. Massachusetts Inst. of Tech., Cambridge, Dept. of Civil Engineering IV. Ulrich Luscher V. DASA WEB No. 13.145 VI. In ASTIA collection</p>	<p>Air Force Special Weapons Center, Kirtland AF Base, New Mexico Rpt. No. AFSWC-TDR-63-6. STUDY OF THE COLLAPSE OF SMALL SOIL-SURROUNDED TUBES. Interim Report, March 1963. 82 p. incl illus., tables, 7 refs. Unclassified Report</p>	<p>This report describes a program of experimental and theoretical work on the problem of failure of structural tubes surrounded by a thin layer of soil loaded by uniform radial outside pressures. The properties and the thickness of the soil layer were varied, and the failure pressure of the tube, as well as the deformations of the tube before and after failure, was observed. Theories based on idealized models of the soil-structure interaction were developed. The experimental results were then correlated with these theories</p>					

	<p>to determine which, if any, of the theories explained the behavior of the samples.</p> <p>In addition to this work, a new testing apparatus was designed and built, in preparation for similar tests with the tube buried under a plane soil surface.</p>		<p>to determine which, if any, of the theories explained the behavior of the samples.</p> <p>In addition to this work, a new testing apparatus was designed and built, in preparation for similar tests with the tube buried under a plane soil surface.</p>
	<p>to determine which, if any, of the theories explained the behavior of the samples.</p> <p>In addition to this work, a new testing apparatus was designed and built, in preparation for similar tests with the tube buried under a plane soil surface.</p>		<p>to determine which, if any, of the theories explained the behavior of the samples.</p> <p>In addition to this work, a new testing apparatus was designed and built, in preparation for similar tests with the tube buried under a plane soil surface.</p>